
ROCK BED STORAGE PERFORMANCE - ARLINGTON SOLAR HOUSE

BY

ROBERT WAYNE PERSONS III

MASTER OF SCIENCE
(MECHANICAL ENGINEERING)

UNIVERSITY OF WISCONSIN-MADISON

1978

ROCK BED STORAGE PERFORMANCE -- ARLINGTON SOLAR HOUSE

BY

ROBERT WAYNE PERSONS III

A thesis submitted in partial fulfillment of the
requirements for the degree of

MASTER OF SCIENCE
(Mechanical Engineering)

at the

UNIVERSITY OF WISCONSIN -- MADISON

1978

ABSTRACT

Operation of the rock bed in the University of Wisconsin Solar Energy Laboratory's Arlington House is compared to the performance as modelled by the TRNSYS transient system simulation program. The model is tested for simulation of temperature profile during short-term (3-8 hr) experiments and energy flow over a longer period (2 weeks).

Temperature profile simulation is accurate within 5% based on internal energy change. Energy flows predicted by simulation are within 5% of measured flows over the long-term test period.

The causes and effects of non-uniform flow distribution in rock beds and suggestions for designing beds with low leakage and uniform flow are also discussed.

ACKNOWLEDGMENT

I am grateful for the growth-inducing challenge, thoughtful evaluation, and warm encouragement which have been provided at the University of Wisconsin Solar Energy Laboratory by Professors J.A. Duffie, W.A. Beckman, J.W. Mitchell, and S.A. Klein. The brainstorming and camaraderie shared among the students and staff of the Lab has also been an important part of my research experience. In particular I am indebted to Jeff Jurinak for his constant reinforcement, and to Dan Erdmann for his assistance with the house, the data, and the enjoyment of life. Finally, I am grateful to my parents for all the effort which they invested in getting me off to a good start.

~~This work has been supported by the Solar Heating and Cooling Research and Development Branch, Office of Conservation and Solar Applications, U.S. Department of Energy.~~

TABLE OF CONTENTS

| | |
|---|----|
| List of Figures | 4 |
| List of Tables | 5 |
| Summary | 6 |
| Introduction | 8 |
| 1.0 Literature Review | 10 |
| 1.1 Development of the Analytical Solution | 10 |
| 1.2 Numerical Adaptations | 11 |
| 1.3 Experimental Work | 13 |
| 2.0 Physical Description and Thermal Performance | 16 |
| 2.1 The Arlington House System | 16 |
| 2.2 Rock Bed Structure, Instrumentation, and Controls | 16 |
| 2.3 Idiosyncracies in the System and the Data | 22 |
| 2.4 Thermal Performance | 25 |
| 2.4.1 Short-term Experiments | 25 |
| 2.4.2 Long-term Performance | 32 |
| 3.0 Short-term Simulation Testing | 37 |
| 3.1 Method of Short-term Testing | 37 |
| 3.2 Comparison of Predictions with Measurements | 39 |
| 4.0 Long-term Simulation Testing | 46 |
| 4.1 Method of Long-term Testing | 46 |
| 4.2 Interval Selection and Data Reduction | 48 |
| 4.3 Analysis of Long-term Results | 49 |
| 5.0 Design Observations | 52 |
| 5.1 Analysis of Flow Distribution | 52 |
| 5.2 Causes and Effects of Non-uniform Flow | 53 |
| 5.3 Design for Uniform Flow | 61 |
| 5.4 Leak Prevention | 63 |
| Recommendations for Future Work | 64 |
| Appendix A Calculation of Heat Transfer Coefficient | 66 |
| Appendix B Arlington House Rock Bed Specifications | 69 |
| Appendix C Nomenclature | 70 |
| Appendix D References | 72 |
| Appendix E Computer Program Listings | 75 |

LIST OF FIGURES

Figure

- 2.1.1 Arlington House System Schematic 17
- 2.2.1 Rock Bed Details 18
- 2.2.2 Stack and Node Representations of the Rock Bed 21
- 2.4.1 Temperature Profile Histories for Short-term Experiments 29
- 2.4.2 Stack Temperature Profile Histories for Experiment CHG2 31
- 2.4.3 Histograms of Rock Bed Inlet and Outlet Air Temperatures 33
- 3.1.1 Finite Difference Infinite Ntu Algorithm 38
- 3.2.1 Temperature Profile Simulations for Short-term Experiments 40
- 3.2.2 Effect of Non-uniform Air Flow on Simulation Results 44
- 4.1.1 Long-term Simulation Testing Method 47
- 5.1.1 Rock Bed Air Flow Distribution 54
- 5.2.1 Control Lag Effect 57
- 5.2.2 System Models for Simulation of Non-uniform Air Flow 59
- A.1 Calculation of Heat Transfer Coefficient 68

LIST OF TABLES

Table

| | | |
|-------|---|----|
| 1.3.1 | Comparison of Pressure Drop and Volumetric Heat Transfer Coefficient Measurements with Correlations | 14 |
| 2.4.1 | Summary of Short-term Experiments | 26 |
| 2.4.2 | Summary of Long-term Performance | 35 |
| 3.2.1 | Accuracy of Short-term Simulations | 42 |
| 4.3.1 | Accuracy of Long-term Simulations | 49 |
| 5.2.1 | Effect of Rock Bed Flow Distribution on System Performance: One-month Simulations | 60 |

SUMMARY

The thermal performance of the Arlington House rock bed storage unit has been studied through several short-term experiments of three to eight hours duration, detailed analysis of two weeks of system data, and statistical analysis of inlet and outlet temperatures over a heating season. The bed stratifies well although a well-defined temperature wave, or thermocline, is not always apparent in the temperature profile. Energy is always available from the top of the bed at temperatures near those received from the collectors and the furnace, while the temperature at the bottom of the bed rarely exceeds 35°C (95°F). Leakage to or from the bed is practically zero. The storage efficiency of the bed is about 90%.¹

The Infinite Ntu rock bed model used in TRNSYS has been tested for accuracy in simulating changes in the bed temperature profile for the short-term experiments and storage and discharge energy flows over the two-week period. Air flow through the bed is substantially non-uniform, thus it does not satisfy the one-dimensional flow assumption of the Infinite Ntu (and almost any other) rock bed model. In spite of this fact, TRNSYS simulations modelled temperature profile change within 5% accuracy based on internal energy change. The Infinite Ntu model also simulated performance of the rock bed over the two-week period with an accuracy of five per cent with respect

¹Storage efficiency \equiv (Energy discharged)/(Energy stored). Note that storage efficiency depends on control strategy and weather.

to the energy flows measured over the same period. A modified simulation was used to show that it would be worthwhile to include convection losses from the rock bed plenum chambers in the model if an accurate accounting of losses is considered important.

Additional simulations have shown that uniformity of air flow does affect the accuracy of rock bed simulation, and that non-uniform air flow in real rock beds may be detrimental to system performance if the thermocline reaches the bottom of high-flow areas of the bed. The relationship between inlet air velocity pressure and pressure drop through the rock bed has been shown important in insuring uniform air flow through beds. A construction method for minimizing air leakage to and from the rock bed has also been described.

INTRODUCTION

Air-based systems with rock bed storage are appropriate for solar residential space heating. In an air-based system, air is used for both collection and delivery of heat. This integrity makes possible simple system designs without the need for antifreeze or drain-down provisions in locations where hydronic systems might freeze, and without the losses associated with storage and delivery heat exchangers. Rock beds exhibit temperature stratification, storing energy at the high outlet temperatures of collectors while simultaneously returning cool air to maximize collector efficiency. Rock beds are easy to design and build, and the necessary materials are widely available. The use of rock beds in solar systems has not been studied in sufficient detail to compare their performance to predictions by mathematical models.

The goals of this study are:

- 1) to evaluate the accuracy of the TRNSYS transient system simulation program in modelling rock bed performance, and
- 2) to relate some observations on rock bed design.

The model evaluation is performed by comparing the predictions of the TRNSYS Infinite Ntu rock bed model to the performance during short- and long-term experiments of a real solar space and water heating system. The short-term tests entail comparison of simulated and measured temperature profiles. The long-term test checks the accuracy of TRNSYS in simulating the storage and discharging energy flows to and from the bed. The real system used for comparison is

the Solar Energy Laboratory's Arlington House. It is a single family residence heated by Owens-Illinois evacuated tubular collectors and an off-peak electric furnace. A schematic diagram of the system is shown in fig. 2.1.1. The collector-to-storage, collector-to-load, and storage-to-load modes of the system are like those for most other air-based space heating systems. The auxiliary-to-storage mode is unique, storing energy during utility off-peak periods for later use.

The design observations included in this study are based on experience with the Arlington House rock bed and other rock beds. They include observations on the significance and achievement of uniform air flow distribution through the rock bed and means of preventing air leakage.

~~Five chapters follow this introduction. First is a brief review~~ of the analytical and numerical solutions of the packed bed heat exchanger problem and prior and current experimental work. Next is a description of the Arlington House rock bed and its thermal performance. Then short-term and long-term simulation accuracies are evaluated in separate chapters. Finally, design observations are reported.

1.0 LITERATURE REVIEW

Published research on packed bed thermal storage and its application to solar heating includes an analytical solution, several numerical adaptations, and some experimental investigations.

1.1 Development of the Analytical Solution

The original theoretical work in packed bed heat transfer was done by Schumann [24]¹ and extended by Furnas [8]. Schumann was motivated by the industrial uses of packed beds, but his solutions apply as well to solar thermal storage. In order to state the problem symbolically, Schumann implicitly assumes a loss-free bed with one-dimensional flow and zero net mass transfer, and makes these explicit assumptions:

- 1) The temperature ~~within each bed particle~~ is uniform.
- 2) The convection heat transfer between the fluid and the bed is much greater than the conduction heat transfer within the fluid or between the bed particles.
- 3) The heat transfer rate between the fluid and the bed is in proportion to the temperature difference between them.
- 4) Material properties are constant with respect to temperature.

Schumann states the equations governing bed and fluid temperatures

as:²

$$\rho_b c_b (1-\epsilon) \frac{\partial T_b}{\partial \theta} = h_v (T_f - T_b), \text{ and} \quad (1.1.1)$$

$$\rho_f c_f \epsilon \frac{\partial T_f}{\partial \theta} + G c_f \frac{\partial T_f}{\partial x} = -h_v (T_f - T_b). \quad (1.1.2)$$

¹ References are listed in Appendix D.

² Nomenclature is defined in Appendix C.

Next, presuming boundary conditions of uniform initial bed temperature and step inlet fluid temperature, he solves the equations and presents solutions for bed and fluid temperatures graphically as temperature difference ratios in terms of dimensionless time and distance.

Furnas [8] uses a graphical integration method to extend Schumann's solutions beyond the range allowed by the Bessel functions which had been tabulated by the time of their work. He also demonstrates the graphical method by which the solutions can be used to calculate, from experimental data, the volumetric heat transfer coefficient for a bed.

1.2 Numerical Adaptations

~~A rock bed is an intermittent heat exchanger -- it cannot store and discharge energy simultaneously. Thus its performance necessarily involves transients and it is rarely at the uniform temperature presumed as an initial condition by Schumann. Most theoretical work on rock beds has been aimed at the numerical simulation of their performance during multiple storage-discharge cycles, and evaluating the effects of relaxing some of Schumann's assumptions.~~

Numerous authors (e.g. refs. 2, 7, 23) have written the Schumann equations in finite difference form. Such models produce very accurate results, but require too much computation for use in long-term system simulations.

Klein [18] discusses the problems inherent in developing a

simple, accurate rock bed model for use in simulations. Hughes [11] and Kuhn et al. [1] describe early attempts to develop such a model. An obvious simplification of the Schumann model for use with air-based systems is the assumption of zero fluid thermal capacitance, allowing omission of the first term in eq. 1.1.2.

Hughes et al. [13] describe the development of the model which is the basis for the TRNSYS rock bed component, and which is tested in the present work. Equations 1.1.1 and 2 (without air capacitance) are expressed in terms of Ntu, the number of heat transfer units comprising the rock bed.

$$\frac{\partial T_f}{\partial (x/L)} = Ntu(T_b - T_f) \quad (1.2.1)$$

$$\frac{\partial T_b}{\partial (\theta/\tau)} = -Ntu(T_b - T_f) \quad (1.2.2)$$

The number of transfer units is a dimensionless expression of the size of a heat exchanger, defined as:

$$Ntu = h A_{fr} L / \dot{m} c_f.$$

Next the modified Ntu of Jeffreson [14], called Ntu_c , is substituted for Ntu in eqs. 1.2.1 and 1.2.2 to allow relaxation of assumptions 1 and 2 of section 1.1. Ntu_c is defined as:

$$Ntu_c = \left\{ \frac{d_s}{L(Pe)} + \frac{(1+Bi/5)}{Ntu} \right\}^{-1},$$

and is only slightly less than Ntu for typical residential and larger solar storage units. System simulations using the resulting pair of coupled differential equations reveal that long-term system

performance becomes insensitive to Ntu_c for values greater than about ten. The modified Ntu for the Arlington House rock bed is 21, and most realistically sized rock beds are expected to satisfy the assumption that Ntu_c is greater than ten. Hughes et al. [13] observed that if Ntu_c is assumed infinite, the pair of coupled equations reduce to a single equation since $T_b = T_f$ throughout the bed. Thus,

$$\frac{\partial T}{\partial (\theta/\tau)} = -L \frac{\partial T}{\partial x} + \frac{UPL}{\dot{m}c_f} (T_{env} - T) \quad (1.2.3)$$

if a term is included to account for losses to the environment. This simplification results in an "Infinite Ntu " model which is economical enough for use in system simulations and accurate for rock beds with Ntu_c greater than ten. As discussed in the introduction, the following chapters test the Infinite Ntu model against the measured thermal performance of the Arlington House rock bed.

1.3 Experimental Work

Most prior experimental work on rock bed thermal storage at the low temperatures and flowrates of solar applications has been aimed at deriving correlations for pressure drop (Δp) and volumetric heat transfer coefficient (h_v). Table 1.3.1 is a comparison of the values of these parameters measured for the Arlington House rock bed with the values predicted by the correlations of various authors. The "measured" value of h_v reported in the table is calculated by comparison of experimental data with the analytical solution of Schumann. (See Appendix A)

Table 1.3.1 Comparison of Pressure Drop and Volumetric Heat Transfer Coefficient Measurement with Correlations

| Method | Δp | | h_v | |
|------------------------|------------|---------------------|--|--|
| | Pa | in H ₂ O | $\text{kJ/hr-m}^3\text{-}^\circ\text{C}$ | $\text{Btu/hr-ft}^3\text{-}^\circ\text{F}$ |
| Current rock bed | 11.2 | (0.045) | 2700 | (40.3) |
| Alanis et al. [1] | - | - | 5530 | (82.5) |
| Close [3] | 5.73 | (0.023) | - | - |
| Furnas [8] | - | - | 6670 | (99.6) |
| Hollands and Pott [10] | 10.2 | (0.041) | 4900 | (73.1) |
| Kays and London [17] | 3.24 | (0.013) | 3930 | (58.7) |
| Löf and Hawley [21] | - | - | 3800 | (56.7) |

The pressure drop correlation of Hollands and Pott compares well with the current experiment. Their correlation is expressed as:

$$\Delta p = \frac{f A_s G_c^2}{2 \rho_f g_c A_c}$$

where the friction factor takes the form of the Ergun correlation with new coefficients:

$$f = 1.27 + 210/\text{Re}_D$$

The wide range of values shown for h_v is mainly of academic interest since any value greater than

$$h_{v,\text{critical}} = \frac{10 \dot{m} c_f}{A_{fr} L}$$

will result in an Ntu greater than ten. Thus, as discussed in the preceding section, long-term system performance will be independent of h_v . For the Arlington House rock bed, $h_{v,\text{critical}}$ is

1200 kJ/hr-m³-°C (17.9 Btu/hr-ft³-°F) and less than half of the measured coefficient. Most rock beds large enough for practical application in solar systems are expected to have h_v greater than $h_{v,critical}$.

Pfannkuch and Edens [22] have compiled data on rock heat capacity and find

$$c_b = 0.0413 T^{0.515} \quad (T \text{ in } ^\circ\text{K})$$

applicable to average polymineral aggregate rocks. This corresponds to a heat capacity of 0.82 kJ/kg-°C (0.20 Btu/lbm-°F) at 60°C with variation of ±6% over the range of 20 to 100°C. Simulations executed for the current work use a constant heat capacity of 0.82 kJ/kg-°C.

Karaki et al. [16] have observed the performance of the rock bed storage unit in Solar House II at Colorado State University. Their report includes a detailed description and illustrations of the construction of the rock bed, and time sequences of temperature profiles for the central stack in the bed.

Jones [15] has instrumented a rock bed for trial application of the ASHRAE Thermal Storage Testing Procedure. He has mentioned problems with air leakage and accurate measurement of humidity of the inlet and outlet air streams.

2.0 PHYSICAL DESCRIPTION AND THERMAL PERFORMANCE

2.1 The Arlington House System

The rock bed under study is part of an air-based space and domestic water heating system located in a residence at the University of Wisconsin's Arlington Experimental Farm. A schematic diagram of the system and a list of its modes of operation is shown in fig.

2.1.1. For a detailed description of the system see Hughes et al.

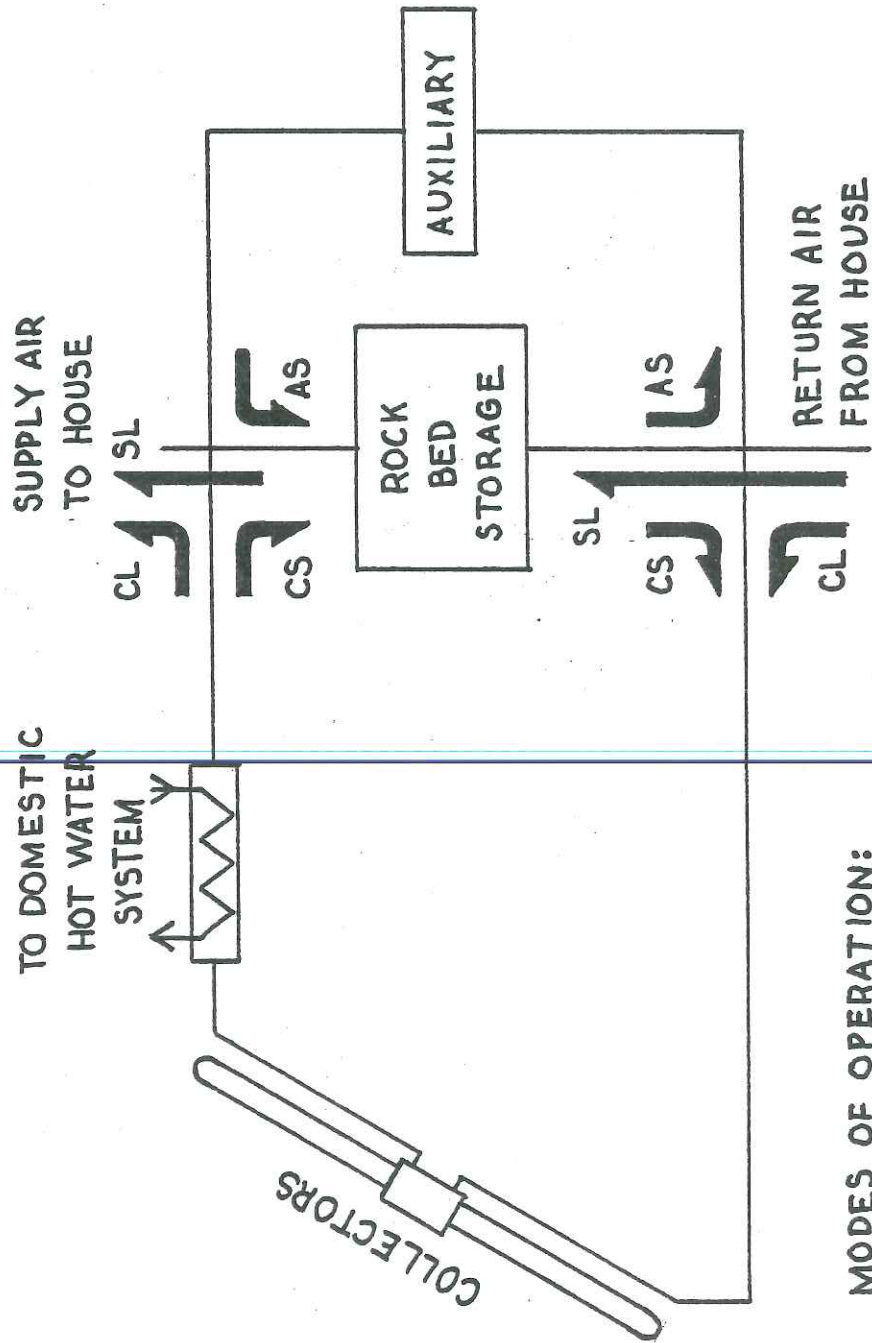
[12], Erdmann [5], and Erdmann and Persons [6]. The house is a detached single family dwelling of 210 m^2 (2250 ft^2) floor space

including the heated basement. The collectors are 380 Owens-Illinois evacuated tubes, manifolded with series pairs in parallel. The modified Solaron air handler circulates 1400 to $2200 \text{ m}^3/\text{hr}$ (860 to 1280 cfm) through the rock bed depending on system mode. The

auxiliary space heating furnace is a 45 kW electric resistance duct unit which operates in five stages of 9 kW each.

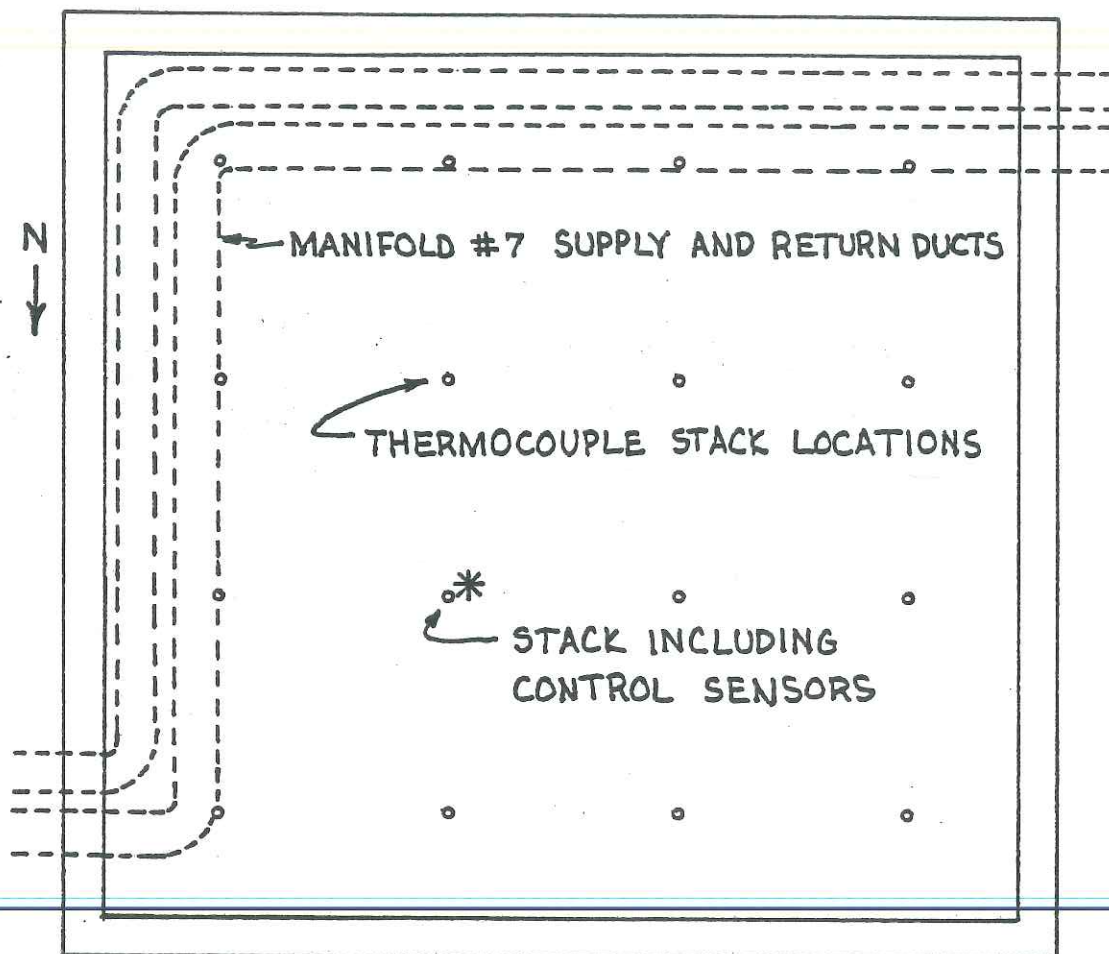
2.2 Rock Bed Structure, Instrumentation, and Controls

Detailed physical specifications for the rock bed are listed in Appendix B, and its structure is shown in fig. 2.2.1. The bed consists of a mass of rocks with dimensions of approximately $3.4 \times 3.6 \times 1.6 \text{ m}$ ($11 \times 12 \times 5 \text{ ft}$), enclosed in an insulated wood frame box and supported on steel mesh and concrete blocks. The south wall of the bed adjoins the house foundation. The north, east, and west walls are exposed to the basement space to aid return of storage heat loss to the load.

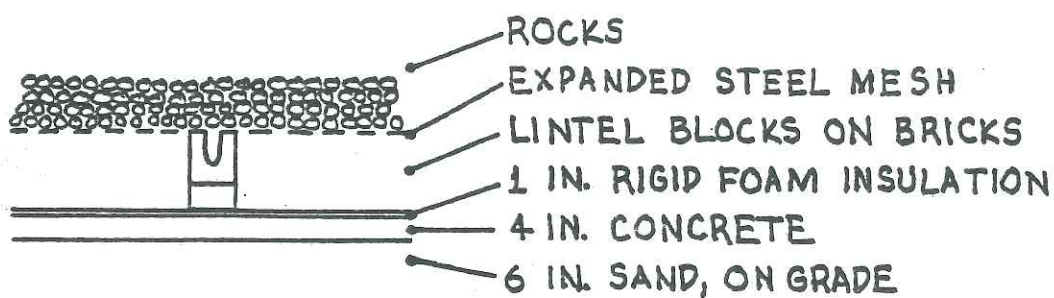


MODES OF OPERATION:
 COLLECTOR - TO - STORAGE (CS)
 AUXILIARY - TO - STORAGE (AS)
 STORAGE - TO - LOAD (SL)
 COLLECTOR - TO - LOAD (CL)

FIGURE 2.11 ARLINGTON HOUSE SYSTEM SCHEMATIC



PLAN VIEW



FLOOR AND LOWER PLENUM CROSS-SECTION

FIGURE 2.2.1 ROCK BED DETAILS

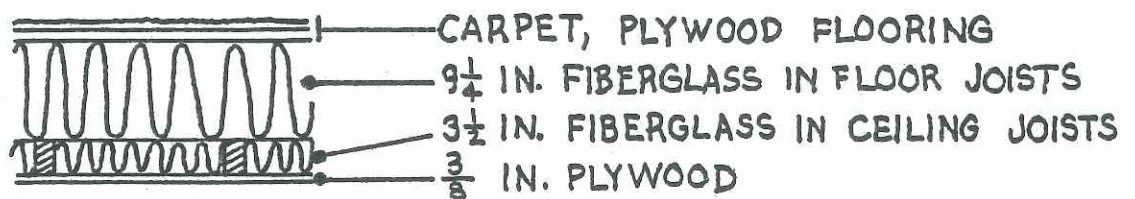
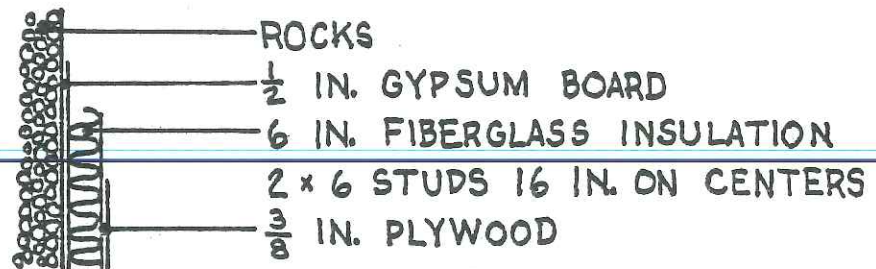
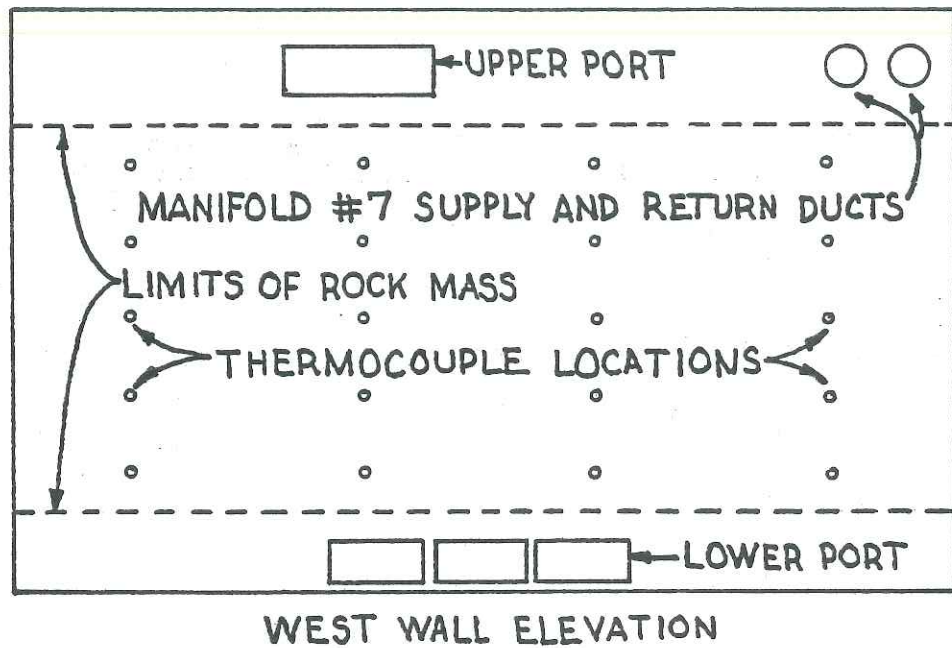
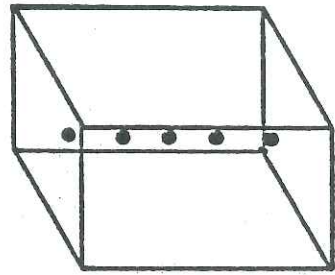


FIGURE 2.2.1 CONTINUED

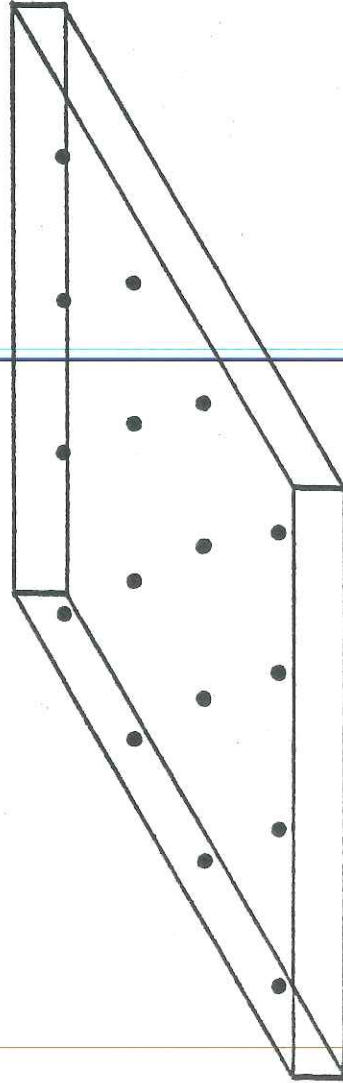
Instrumentation used in the rock bed consists of 82 thermocouples. Two thermocouples placed near the plenum ports measure inlet and outlet air temperatures. Eighty thermocouples are placed in five horizontal four-by-four arrays within the bed as shown in fig. 2.2.1. This arrangement allows modelling of the rock bed as eighty equal volumes, each with a thermocouple at its geometric center. The bed can thus be represented as five horizontal nodes or as a four-by-four array of vertical stacks. These visualizations, illustrated in fig. 2.2.2, are used below in analyzing temperature profiles and flow distributions. The eighty internal thermocouples are crimped and epoxied into three-inch lengths of 1/4 inch diameter copper tubing to insure good thermal contact with rock and represent the average rock temperature at each location. All eighty thermocouples are monitored during short-term experiments, but only one thermocouple at each node can be monitored as part of the long-term system performance data. The five constantly-monitored thermocouples are in the same stack as the control sensors, shown in fig. 2.2.1.

Other system instrumentation used to measure the energy entering and leaving the rock bed includes a furnace power transducer, three air flow meters, and a barometric pressure transducer. The air flow meters each consist of a pneumatically averaging array of Pitot tubes downstream from a honeycomb flow straightener.

Control sensors are placed at intervals of one foot starting one half foot below the rock surface on a vertical line located as shown in fig. 2.2.1. These sensors, with other sensors located in



STACK



NODE

FIGURE 2.2.2 STACK AND NODE REPRESENTATIONS OF THE ROCK BED

the collectors and living space, control fan operation and damper positions to produce the four system modes shown in fig. 2.1.1 and described below.

The air handler circulates air downward through the bed for charging and upward for discharging. This flow routing results in thermal stratification, an essential advantage of rock bed storage as discussed by Klein [18]. The temperature difference between the lower rock bed control sensor and a sensor in a tubular collector annulus is used to control the collector-to-storage (CS) and collector-to-load modes. The average temperature of the five rock bed sensors controls the auxiliary-to-storage (AS) mode, which operates during the utility off-peak hours (10 pm to 8 am). The system has no provision for a direct auxiliary-to-load mode. The storage-to-load (SL) mode is controlled by the load thermostat, and has priority over the AS and CS modes. During summer operation the rock bed is bypassed in a collector-to-water mode.

2.3 Idiosyncracies in the System and the Data

Measurement of the performance of the Arlington House rock bed and comparison of that performance to simulation results require consideration of three peculiarities of the rock bed and system and two limitations on the use of experimental data.

The system peculiarities are non-uniform flow distribution through the rock bed, thermosyphon loss from the rock bed through system ducts, and the absence of a transducer positioned to measure

exactly the air flow rate through the bed. The evidence, causes, and effects of non-uniform air flow distribution in the rock bed are discussed in Section 2.4.1 and Chapter 5. Substantial energy losses due to thermosyphoning from the bed were discovered in January of 1978. Energy was escaping to the outdoors by air circulation between the rock bed and one of the collector manifolds via the manifold supply and return ducts, which pass through the upper plenum of the rock bed as shown in fig. 2.2.1. The problem was discovered when temperature differences of up to 39°C (70°F) between the manifold and ambient air were recorded on cold winter nights, in spite of the thick insulation on the portions of the ducts inside the bed. The problem was virtually eliminated before the data used in this report were collected by the addition of gravity-operated backdraft dampers to the thermosyphoning ducts. Special considerations are necessary with regard to the measurement of air flow through the rock bed in the AS and CS modes. There is no space for a flow transducer in the AS air flow circuit. Therefore AS air flow has been measured by doing a duct traverse with Pitot tube and micromanometer. Data thus measured are less exact than the constantly-monitored velocity pressures available for SL mode operation. Air flow rate in the CS mode is measured both going to and coming from the collectors. Due to air infiltration at the collectors and exfiltration in the ducts and air handler, there is 15 to 20% more air returning from the collectors than is delivered to them. Thus the air flow rate through the rock bed in the CS mode is only known to be less than the return

air flow from the collectors and more than the collector supply air flow, and cannot be measured exactly.

The limitations on the use of data involve the inlet air temperature in the AS mode and the five constantly-monitored rock bed internal temperatures. The upper plenum port thermocouple, which measures T_{in} in the AS mode, is about two feet from the auxiliary furnace coils. Although it is radiation shielded, it indicates an air temperature in the AS mode substantially in excess of the true temperature. Use of a five-thermocouple array at the upper plenum port reveals that the single thermocouple measurement is as much as 17°C (31°F) above the mass average temperature, depending on the number of active furnace stages. This indicates a lack of air mixing between the furnace coil and the thermocouple location, and that the thermocouple is in the streamline of one of the heating coils. But inlet air temperature data are necessary for simulations. Impedance limitations on the datalogger prohibit use of an averaging thermocouple array, so provisions for air mixing would be required for correct measurement of inlet temperature in the AS mode. Fortunately, integrated auxiliary furnace power is available as a redundant measure of the energy flowing into the bed in the AS mode. Inlet temperatures for use in simulations can be estimated by balancing furnace power with the rate of convection heat transfer to the bed.

Temperature data from the five constantly-monitored rock bed internal thermocouples are useless without simultaneous data from the other 75 internal thermocouples due to the non-uniform distribution

of air flow through the bed. The five thermocouples are accurate, but they do not approximate node-average temperatures. This precludes their use in measuring internal energy change in the bed and conduction losses from the bed, and in checking the other means of measuring the energy stored and discharged. Conduction losses can be estimated. Internal energy change remains an unknown which decreases in significance as the term of a performance analysis is increased.

These system idiosyncracies and data limitations have some bearing on the performance analyses and simulations which are used in this study, so means of circumventing them are discussed in the sections and chapters which follow.

2.4 Thermal Performance

Thermal performance of the Arlington House rock bed has been analyzed on the basis of detailed data recorded during several brief (3 to 8 hr) storage and discharge experiments and system data recorded during December of 1977 through April of 1978.

2.4.1 Short-term Experiments

Descriptions and energy balances for four short-term experiments are shown in Table 2.4.1. Energy flow is measured by furnace power consumption,

$$\Delta E_p = \int P d\theta$$

for the charging tests and by air heat flow,

$$\Delta E_f = \int \dot{m} c_f (T_{in} - T_{out}) d\theta,$$

for the discharging tests. Internal energy change,

$$\Delta U = \frac{m_b}{80} \sum_{j=1}^{80} (\int c_b dT)_j$$

is based on temperature change at the internal thermocouples, all eighty of which are monitored during these short-term experiments.

Table 2.4.1 Summary of Short-term Experiments

| Test | Description | Energy stored, GJ | | | Lack of closure, % |
|------|---|-------------------|--------------|------------|--------------------|
| | | ΔE_p | ΔE_f | ΔU | |
| CHG2 | 8 hr 40 min AS from uniform initial temperature | 1.12 | - | 1.19 | -6. |
| AS3 | 3 hr AS | 0.36 | - | 0.36 | -0. |
| AS4 | 3 hr AS | 0.35 | | 0.37 | -6. |
| SL2 | 4 hr SL | - | -0.28 | -0.30 | +7. |

The energy balance lack of closure values shown in Table 2.4.1 are considered sufficiently small to allow evaluation of the accuracy of simulated temperature profiles, but suggest closer scrutiny of the methods used to perform the energy balances.

There are three ways of calculating energy flows to the rock bed in the AS mode: integrated furnace power, internal energy change of the rock bed, and integrated air heat flow. Comparison of the results of the three methods leads to observations important in measurement of long-term thermal performance and in preparation of data for simulations.

Integrated furnace power is the most accurate gauge of energy supplied to the rock bed in the AS mode. Power transducer accuracy

has been verified by comparison to Wisconsin Power and Light Co. data. Thus it is used in long-term performance evaluation as the definitive measure of energy stored in the AS mode. All of the AS mode energy balances in Table 2.4.1 compare integrated furnace power with internal energy change and show negative lack of closure, indicating gains where losses should be expected. This implies that heat capacity has been overestimated in the energy balance calculations. Since no trend is apparent in the lack of closure values, it is impossible to suggest an alternate specific heat. The heat capacity function of temperature used in the energy balances is that of Pfannkuch and Edens [22] discussed in Chapter 1. A revision of their correlation for use with the current rock bed would require a calorimetric analysis over a temperature range of 20 to 100°C of a random sample of rocks from the bed. A revised expression of heat capacity would enable better design and performance analysis, but a sensitivity study indicates that variations of $\pm 6\%$ in heat capacity have a negligible effect on simulation results.

Integrated air heat flow in the AS mode grossly overpredicts energy stored in comparison to the integrated furnace power, due to the inaccuracy of the upper plenum port thermocouple as discussed in section 2.3. For the current work an inlet air pseudo-temperature is calculated to provide data for use in simulations. This calculation is discussed in detail in Chapters 3 and 4.

Figure 2.4.1 illustrates the histories of the node-average temperature profiles in the rock bed for the storage and discharge tests discussed above. The first graph in fig. 2.4.1, for instance, represents the 8 hr 40 min charging test labelled CHG2. The curves shown are the initial (virtually uniform) temperature profile, hourly profiles, and the final profile. Stratification is evident as the 43°C (77°F) temperature difference between the top and bottom nodes. The point of maximum temperature gradient on each curve is called the thermocline, a term which is used below in discussing rock bed performance.

Temperature profile histories for individual stacks of thermocouples during experiment CHG2 are shown in fig. 2.4.2. The differences in profile shape and bottom thermocouple temperature increase reveal that more energy was stored in one stack than in the other. Inlet air temperature in the AS mode is known to be virtually constant across the top face of the rock bed. Therefore the difference between the stacks in energy stored indicates that the air flow within the bed is not uniform in the charging mode. (The stack including the control sensors receives the least airflow of any of the sixteen stacks.) Similar comparisons of discharging temperature profiles show that discharging flow is more nearly uniform. The modelling implications and other effects of non-uniform flow are discussed in later chapters.

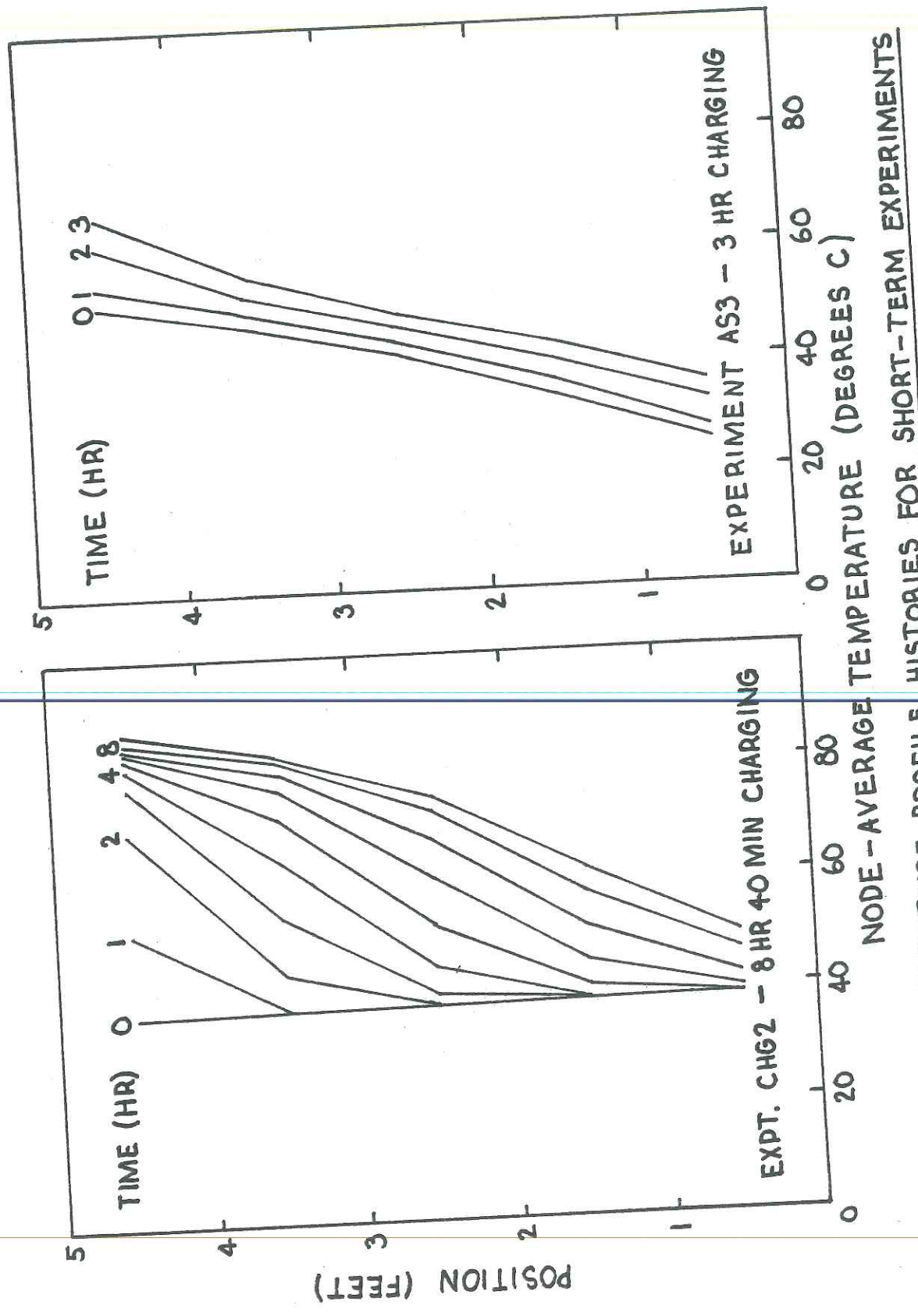


FIGURE 2.4.1 TEMPERATURE PROFILE HISTORIES FOR SHORT-TERM EXPERIMENTS

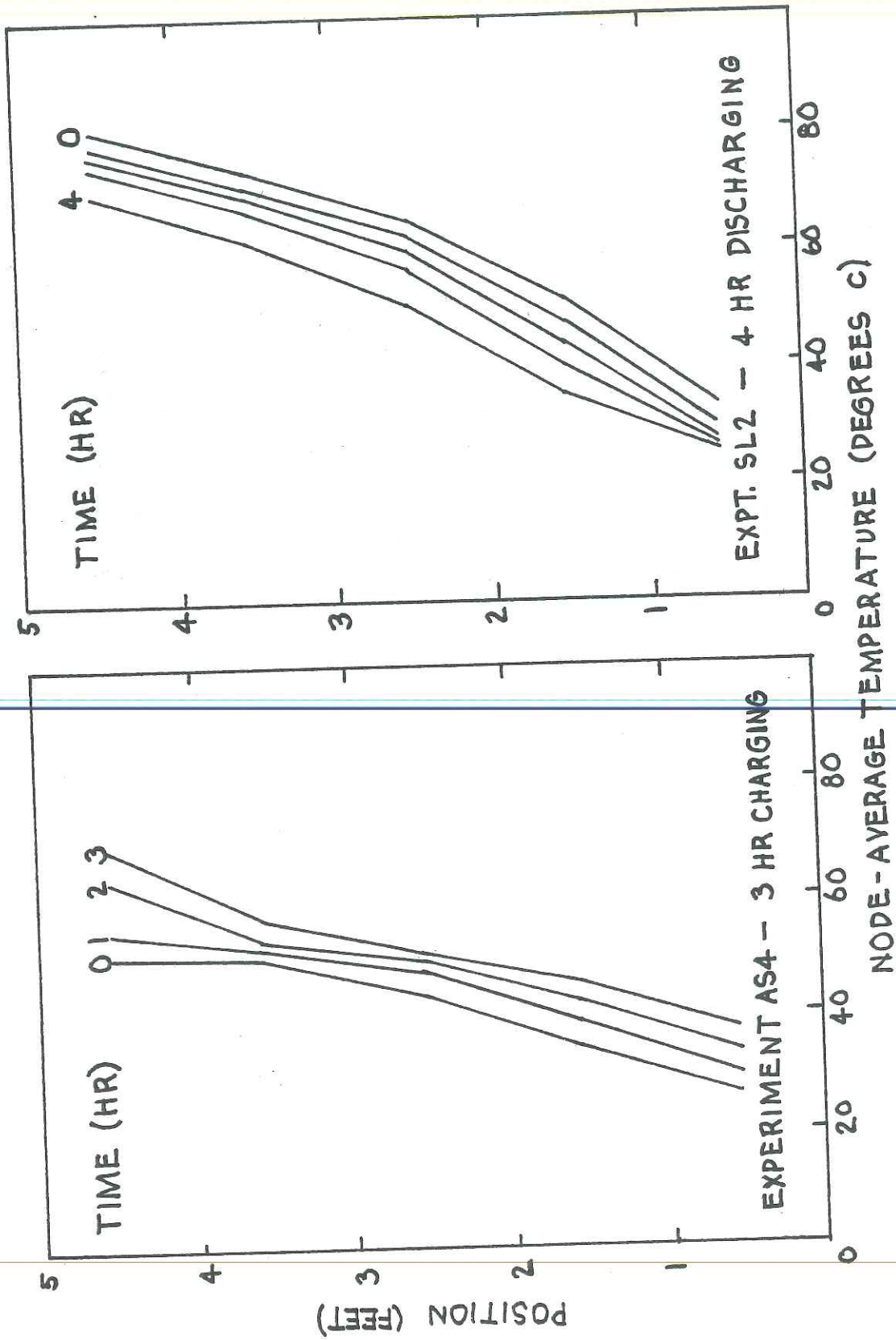


FIGURE 2.4.1 CONTINUED

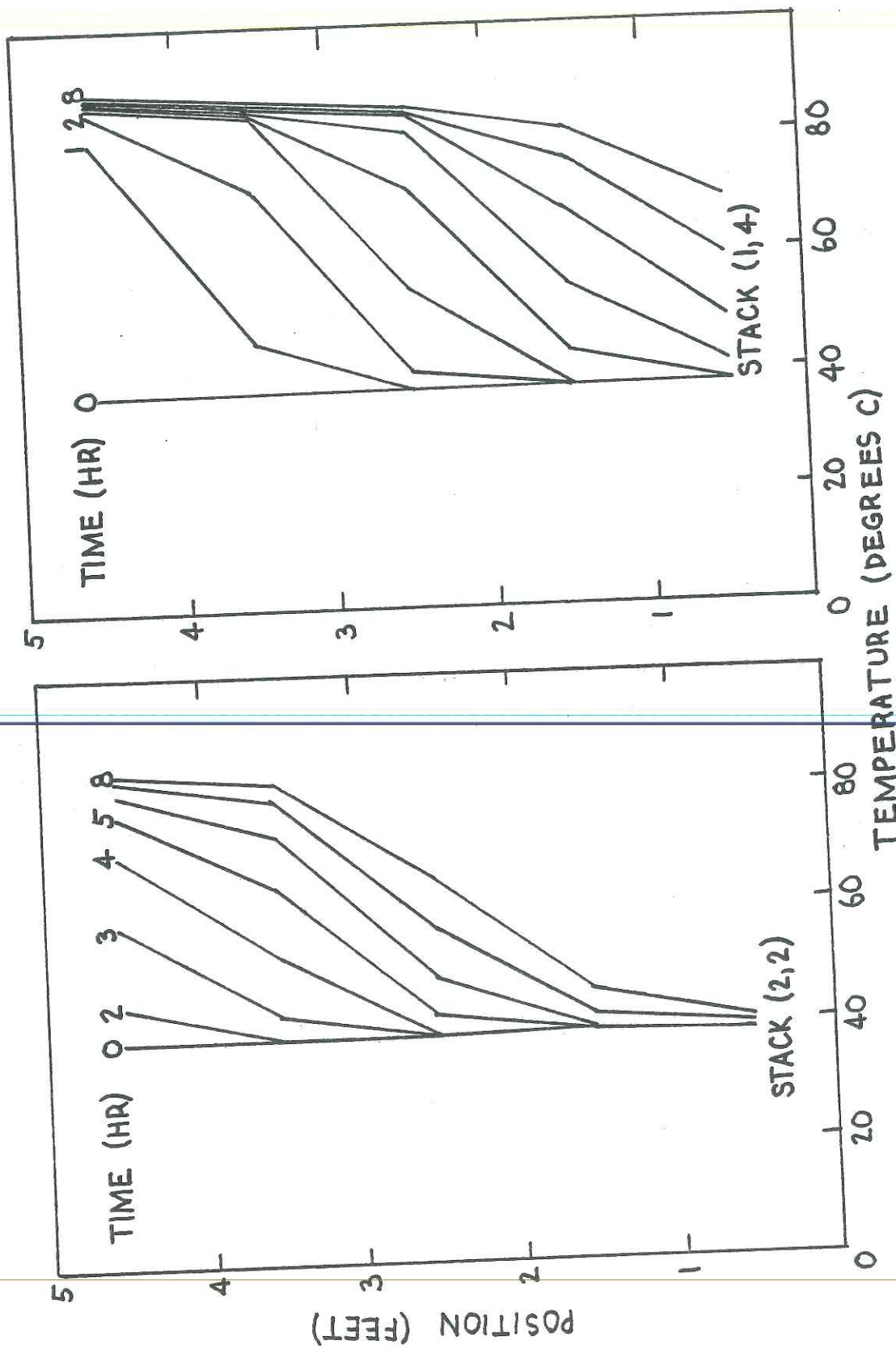


FIGURE 2.4.2 STACK TEMPERATURE PROFILE HISTORIES FOR EXPERIMENT CH62

2.4.2 Long-term Performance

Available data on long-term performance of the rock bed include flowrate through the rock bed, inlet and outlet air temperatures, integrated auxiliary power, and five internal temperatures. All of these data are scanned at ten minute intervals and about 30 seconds after each mode change. The remaining 75 internal temperatures cannot be monitored constantly due to the limited capacity of the datalogger.

Three limitations must be considered in evaluating long-term rock bed performance data, for reasons discussed in section 2.3. First is the inaccuracy of the AS mode inlet air temperature data. Fortunately furnace power data allow accurate measurement of AS energy storage. Secondly, the five constantly-monitored rock bed temperatures cannot be used for measuring internal energy change in the bed or conduction losses from the bed, or for checking the other means of measuring the energy stored and discharged. Conduction losses are estimated for the two-week period of analysis. Internal energy change remains an unknown, but is unlikely to be significant relative to the energy stored and discharged over the two-week period. Finally, due to the absence of a flowmeter immediately upstream or downstream of the bed, it can be said only that the flowrate through the rock bed in the CS mode is bracketed by the collector supply and return flowrates.

Histograms of air temperatures entering and leaving the rock bed in the CS and SL modes are shown in fig. 2.4.3. The CS histogram

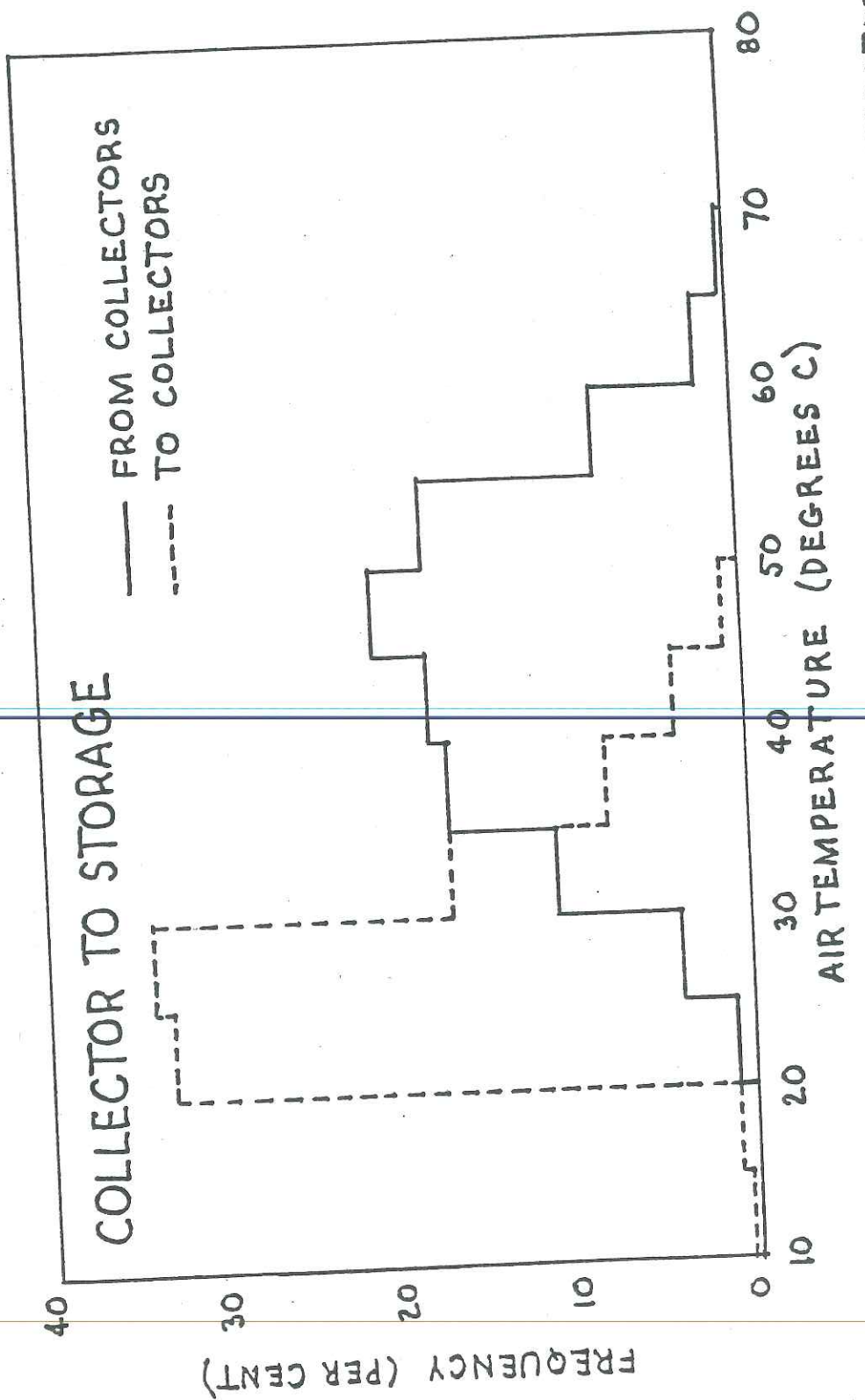


FIGURE 2.4.3 HISTOGRAMS OF ROCK BED INLET AND OUTLET AIR TEMPERATURES

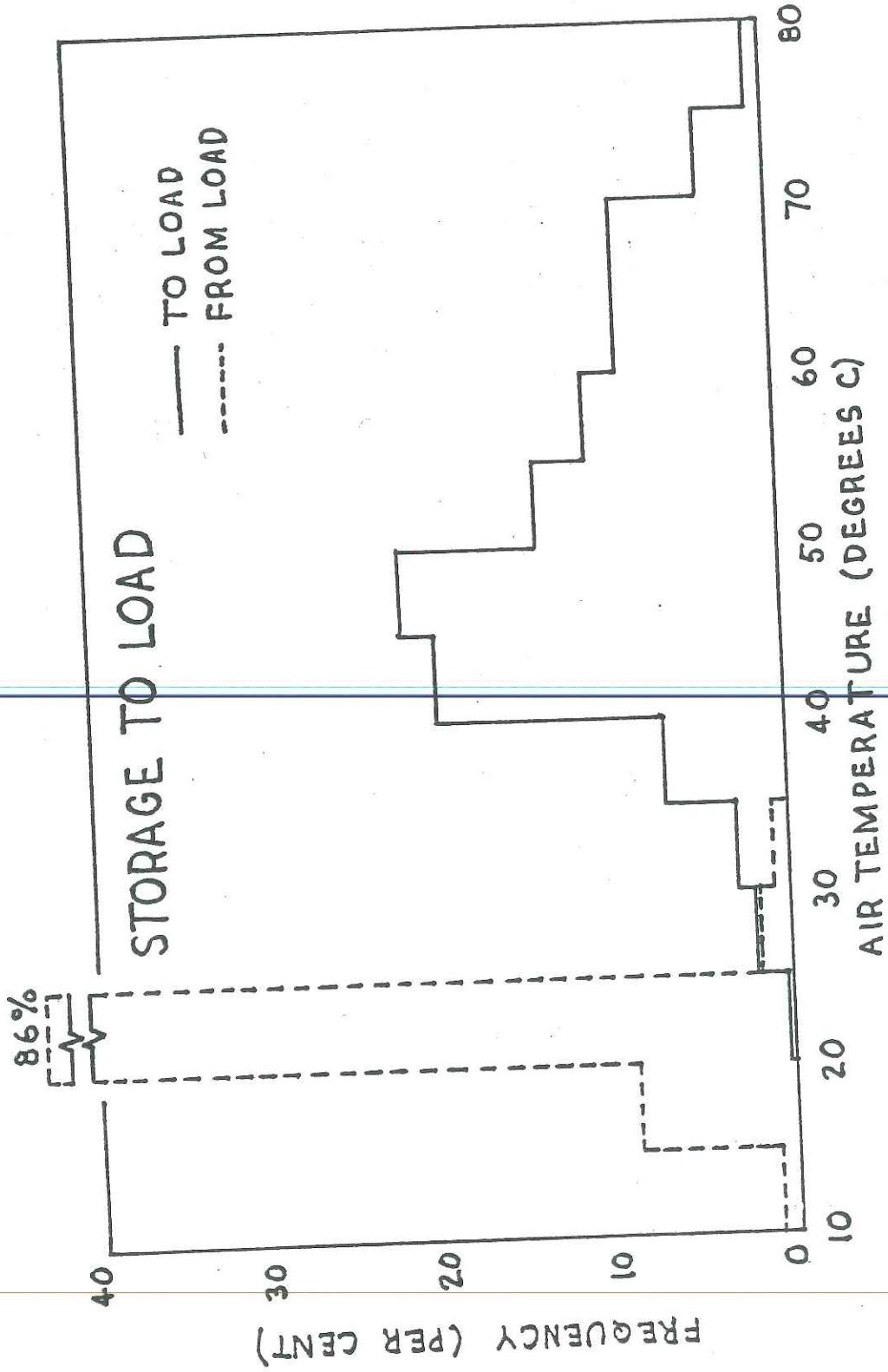


FIGURE 2.4.3 CONTINUED

shows the benefit of stratification. Collector efficiency is enhanced as the hot air received from the collectors returns to them at a much lower temperature. Likewise the SL histogram shows that the high temperatures delivered by the collectors and the furnace are preserved by stratification.

Further observations on long-term rock bed performance are based on a detailed analysis of data recorded during two weeks of system operation in March, referred to as Interval A. This analysis is done using a computer program called RBM, which is included in Appendix E. A conceptual diagram of RBM is shown in fig. 4.1.1. Results of the analysis are shown in Table 2.4.2.

Table 2.4.2 Summary of Long-term Performance

| Energy quantities stored or discharged over two-week test period, | | | | | |
|---|-----------|-----------|----------------------------|---|---|
| by mode, GJ: | | | | | |
| <u>CS</u> | <u>AS</u> | <u>SL</u> | <u>Losses</u> ¹ | <u>ΔU</u> ² | <u>Σ</u> ³ |
| 1.98 to 2.36 | 1.48 | 3.34 | 0.69 | ? | -0.57 to -0.19 |

Notes: ¹Upper bound estimate
²Unknown -- see text
³ $\Sigma = CS + AS - SL - \text{Losses}$

A useful basis for evaluating the results shown in the table is the sum of energy stored in the CS and AS modes. Storage efficiency ($SL / (CS + AS)$) is then between 87 and 97%, subject to the uncertainties in ΔU and the energy stored in the CS mode. If the normally monitored temperature profiles were meaningful, they would show an internal energy increase over Interval A of 0.17 GJ. That is about five per cent of the energy stored over the interval, and would imply an increase in storage efficiency.

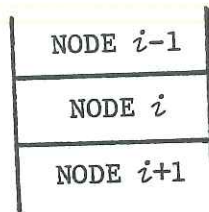
Two mechanisms contribute to losses from the rock bed: conduction losses to its surroundings and air leakage at joints. Losses for Interval A were about 10% of the energy which entered the bed during that period. The upper bound estimate of conduction loss shown in Table 2.4.2 would account for twice that amount. Thus conduction is believed responsible for most heat loss from the rock bed. About 60% of the convection loss is to the ground and outside air, the remaining 40% is to the basement. Air leakage is estimated to be less than two per cent of the energy entering the bed. Severe leakage was noticed and repaired during preliminary operation of the system. Methods of preventing leakage are discussed in Chapter 5.

3.0 SHORT-TERM SIMULATION TESTING

It should be possible to use a rock bed model to simulate temperature profile variation over several hours of system operation, and to simulate energy flows over weeks and months. The accuracy of the TRNSYS rock bed model in simulating long-term performance is discussed in Chapter 4. The goal of this chapter is to determine whether the TRNSYS model is also useful in short-term temperature profile simulation. Short-term accuracy would, for instance, enable one to observe the effect on stratification of varying the simulation parameters, or observe thermocline position in order to aid bed sizing and choice of control criteria.

3.1 Method of Short-term Testing

The Infinite Ntu model was tested using the parameters for the Arlington House bed, for which Ntu_c is 21. The finite difference algorithm used to implement the infinite Ntu method, as expressed by eq. 1.2.1, is illustrated in fig. 3.1.1. The program used for short-term simulation is called FDTIN, and is listed in Appendix E. FDTIN is like the TRNSYS rock bed model, but has simplified input, output, and executive sections to minimize computing costs. The executive section uses a simple Euler scheme to integrate the energy rate at each node. The Euler scheme is less sophisticated than the predictor-corrector integration scheme used in the executive sub-routine of TRNSYS. Justification for use of the Euler scheme is as follows. The timestep in the test data is much less than the critical



For downward air flow
through internal node " i ":

$$\frac{V_b}{N} \rho_b c_b \frac{dT_i}{d\theta} = \dot{m} c_f (T_{i-1} - T_i) - \frac{UPL}{N} (T_i - T_{env}) + \frac{NkA}{L} (T_{i-1} - T_i) - \frac{NkA}{L} (T_i - T_{i+1})$$

FIGURE 3.1.1 FINITE DIFFERENCE INFINITE Ntu ALGORITHM

timestep for the bed model. The critical timestep is

$$\Delta\theta_c = \frac{m_b c_b}{N \dot{m} c_f}$$

Five nodes ($N = 5$) are generally used to simulate the bed, and the maximum air flow rate is about 2400 kg/hr (5300 lbm/hr), so $\Delta\theta_c$ is two hours. Data for storage and discharging tests are taken at 20 minute intervals. Thus a simulation using Euler integration should produce the same results as a simulation using a predictor-corrector integration method. In fact, simulation of a three hour discharging test using FDTIN does predict the same final temperature profile as a TRNSYS simulation using the same data and 20 minute timestep to within 0.1°C at all five points on the temperature profile. For either type of simulation, halving the timestep has a similarly small effect on the results.

The simulations of short-term storage and discharge experiments are initialized with the initial node-average temperature profile

from the experiments, and driven with inlet temperature data from the experiments. The storage experiments were performed in the AS mode. As discussed in section 2.3, the true average inlet air temperature in the AS mode is considerably less than the value detected at the inlet port thermocouple. The inlet temperatures for all timesteps are thus corrected by a term TFIX based on one comparison of integrated air heat flow to integrated furnace power over each experiment.

$$\Delta E_p = \dot{m}c_f \int (T_{in} - T_{out}) d\theta$$

The thermocouple requiring correction in the AS mode accurately measures the inlet temperature in the CS mode and outlet temperature in the SL mode.

The final temperature profiles predicted by FDTIN, using Euler integration and adjusted inlet temperature data, are then compared to the final node-average profiles measured during the short-term experiments.

3.2 Comparison of Predictions with Measurements

Figure 3.2.1 illustrates the accuracy of the infinite Ntu model in simulating the temperature profiles for the short-term experiments described in Chapter 2. Each graph shows rock (and fluid) temperature as a function of position in the rock bed. The three curves shown in each graph are the initial and final measured temperature profiles, and the predicted final profile (dashed line). For the 8 hr 40 min charging test CHG2, the four hour measured and predicted temperature profiles are also shown.

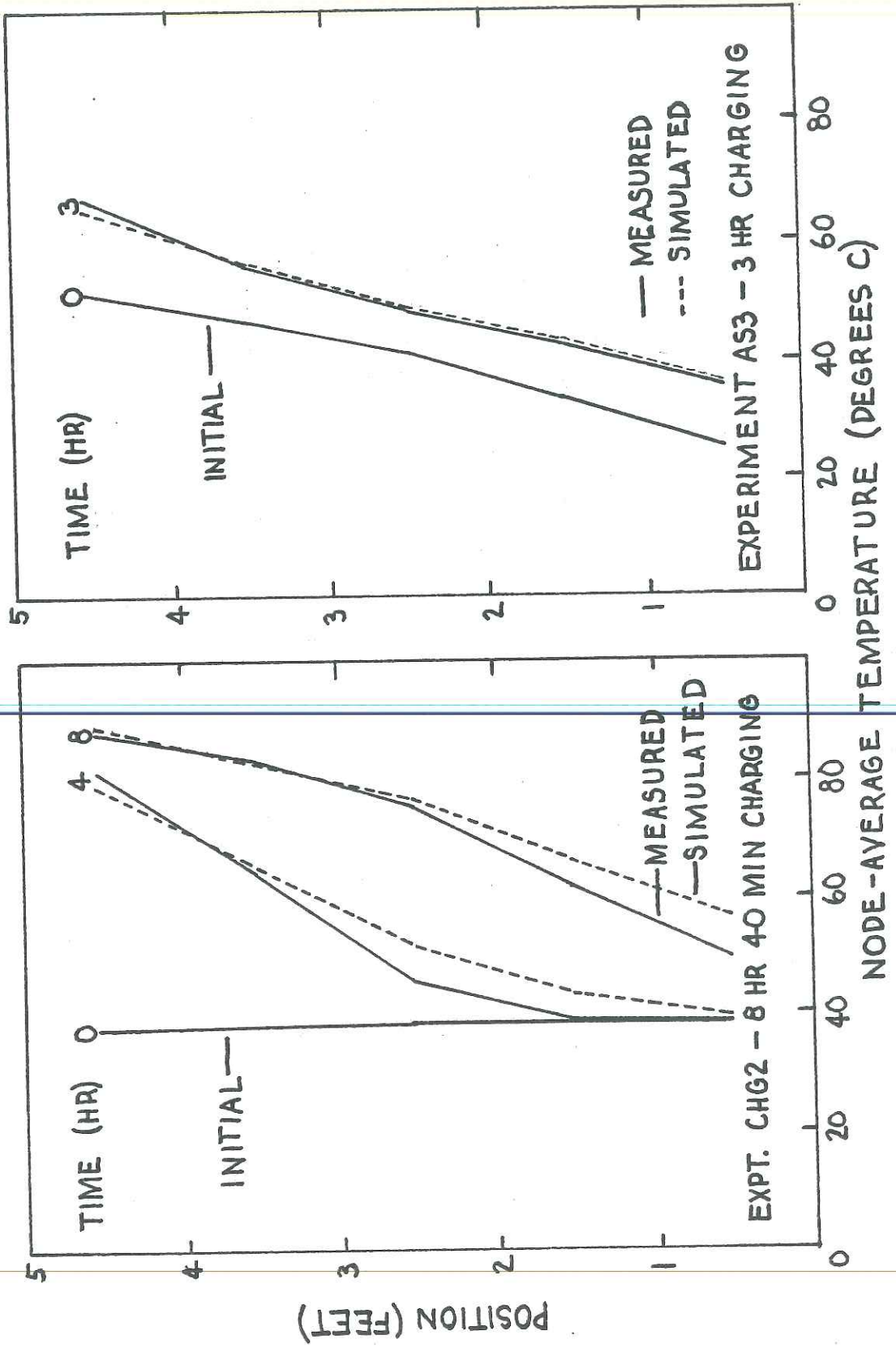


FIG. 3.2.1 TEMPERATURE PROFILE SIMULATIONS FOR SHORT-TERM EXPERIMENTS

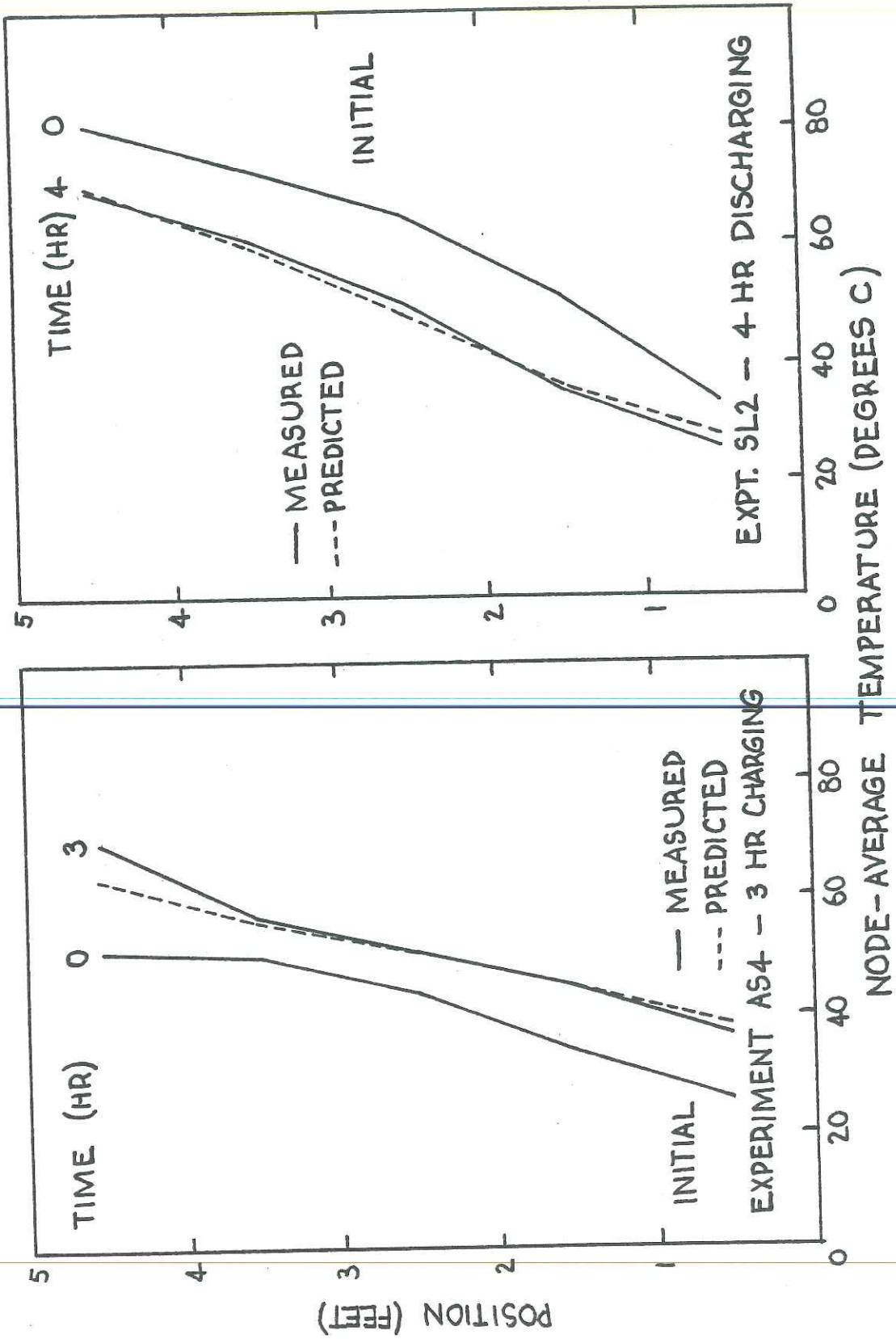


FIGURE 3.2.1 CONTINUED

Qualitatively, the simulated profiles closely approximate the measured profiles. Comparison of the areas between the initial temperature profile and the two final profiles, i.e. of the measured and predicted internal energy changes, is useful as a measure of success in simulation. The areas between the initial and the final profiles must be approximated by rectangular integration since the temperatures at the upstream and downstream faces of the rock bed are unknown. The accuracy of each simulation is represented as

$$\Delta U/U_m = (U_s - U_m)/U_m .$$

The values of $\Delta U/U_m$ for the four tests illustrated in fig. 3.2.1 are shown in Table 3.2.1.

Table 3.2.1 Accuracy of Short-term Simulations

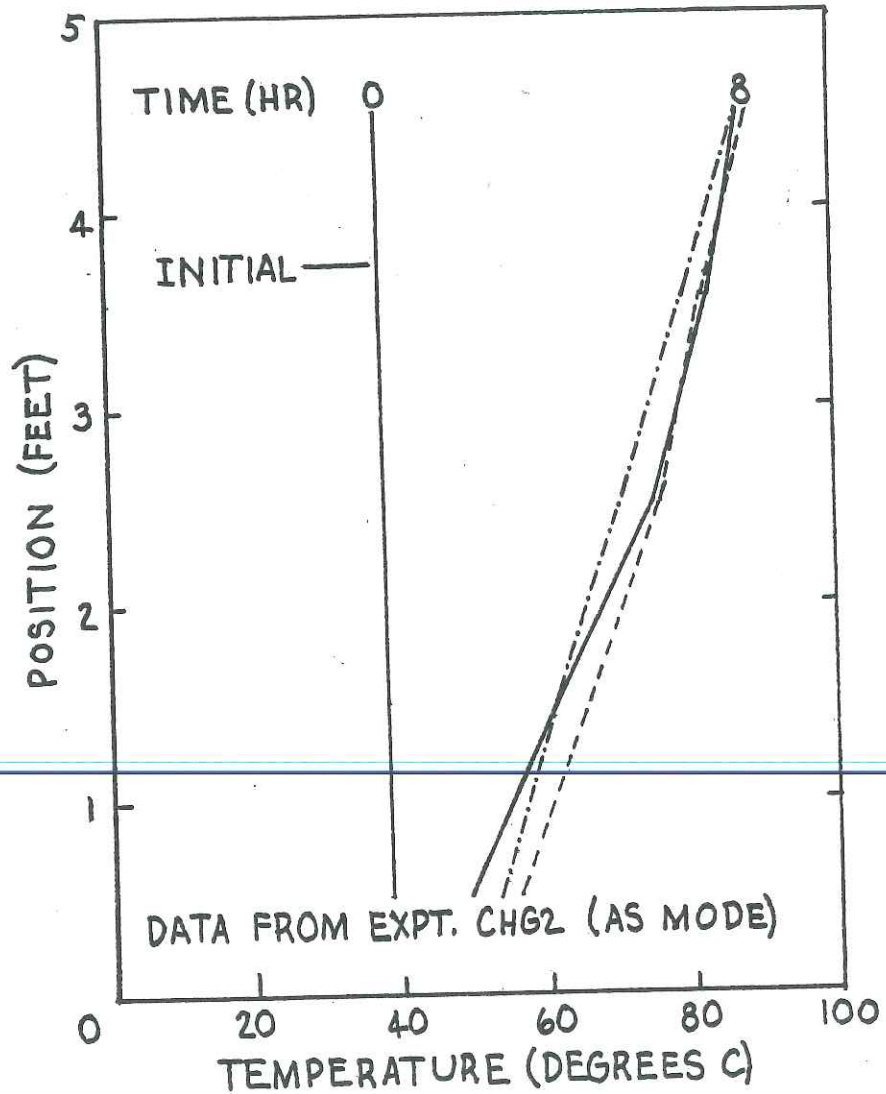
| Test | Mode | $\Delta U/U_m, \%$ |
|------|------|--------------------|
| CHG2 | AS | +7% |
| AS3 | AS | +1% |
| AS4 | AS | -11% |
| SL2 | SL | -2% |

An interpretation of the results shown in Table 3.2.1 must consider the precision levels of the simulation parameters and that the one-dimensional flow assumption of the model is not satisfied during charging of the real rock bed. These considerations are in addition to the implication of the actual finite Ntu discussed above.

Flowrates for the AS tests were measured by performing duct traverses with a Pitot tube and micromanometer. Thus the flowrates

used as inputs to the simulations have a precision of 5%. Rock specific heat varies with mineral type and temperature as discussed in Chapter 1, so the precision of the c_p parameter in the simulations is about 2%. The other parameters are less difficult to measure and probably have a combined precision of less than one per cent. The overall precision of measurement is thus about 8%. This precision level is comparable to the simulation accuracies listed in Table 3.2.1.

The effect of flow uniformity on short-term simulation warrants further discussion. The non-uniformity of flow through the bed in the charging modes has been discussed in Chapter 2 and is considered in more detail in Chapter 5. Using the method described in Chapter 5 it is possible to estimate the distribution of flow among the sixteen stacks in the bed at the upstream face. Assuming one-dimensional flow within each stack, it is possible to predict a final temperature profile for each stack based on its initial profile and flowrate. The effect of non-uniform flow on simulation results may then be assessed by comparing the average of these sixteen final profiles to a profile generated using the node-average initial profile and total flowrate. Such profiles have been generated for experiment CHG2 and are shown in fig. 3.2.2. The average of the sixteen simulated stack final profiles does not match the node-average simulated final profile. The two simulated final profiles do, over most of their lengths, bracket the node-average measured final profile. For the stack-average profile, $\Delta U/U_m$ is -10%.



- MEASURED 8 HR TEMPERATURE PROFILE
- NODE-AVERAGE SIMULATION
- STACK-AVERAGE SIMULATION

FIGURE 3.2.2 EFFECT OF NON-UNIFORM AIR FLOW ON SIMULATION RESULTS

Non-uniform flow may account for the failure of such a linear combination of stack solutions to yield the whole-bed single solution. There are cross flows between stacks and locally low heat transfer coefficients. Airflow which is non-uniform near the upstream face of the rock bed will tend to become more uniform by horizontal dispersion as it travels through the bed. The energy which is thus transferred by convection through the imaginary boundaries of the sixteen stacks in the rock bed is not accounted for by the one-dimensional model.

Thus there is a relationship between flow uniformity within a rock bed and short-term accuracy of the infinite Ntu model. As will be further discussed in Chapter 5, test AS3 exhibits the most nearly uniform flow of any of the charging tests, and discharging flow is ~~very nearly uniform for any SL test.~~ Correspondingly, simulations of experiments AS3 and SL2 show the best agreement with measurement.

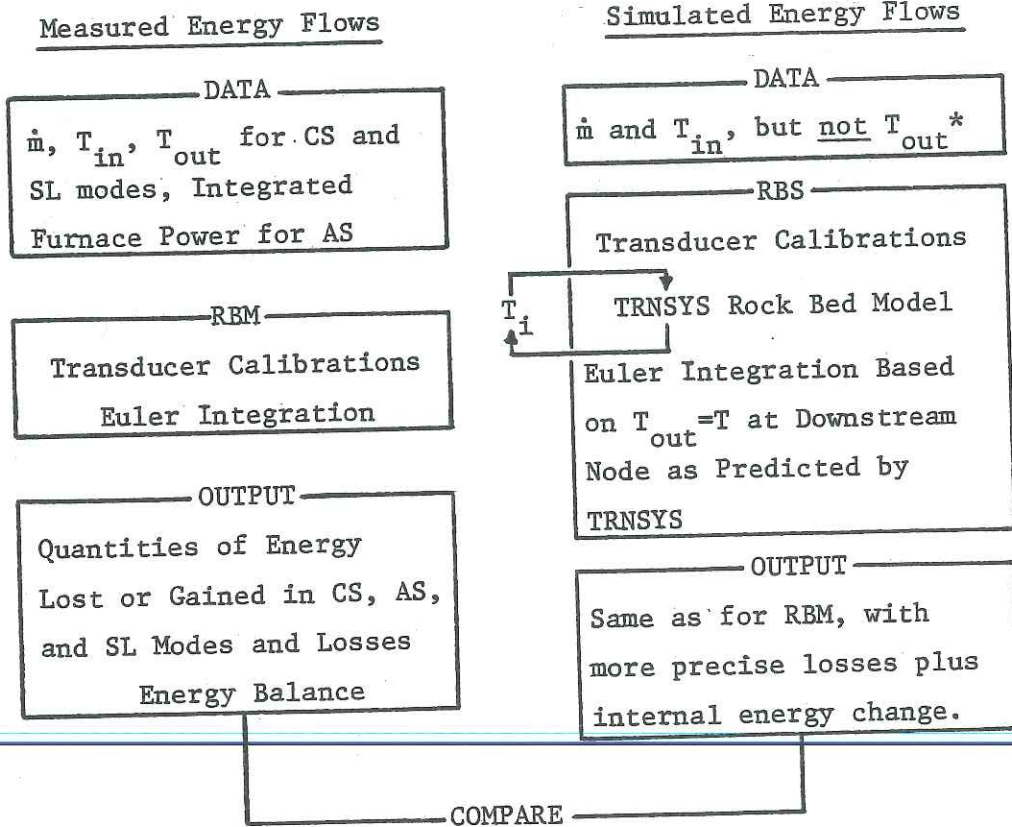
In spite of substantial departure from the one-dimensional flow assumption and uncertainty in some of the parameters, the Infinite Ntu model simulates overall rock bed behavior with about 5% accuracy, sufficient for solar system design applications.

4.0 LONG-TERM SIMULATION TESTING

The most important function of an energy storage component model is the correct representation of the quantities of energy stored and discharged over time periods typical of system simulations, such as weeks or months. This chapter describes a test of that ability in the TRNSYS rock bed model using data from the rock bed at the Arlington House.

4.1 Method of Long-term Testing

A conceptual diagram of the method used for long-term simulation testing is shown in fig. 4.1.1. The test requires comparison of measured and simulated energy flows in each mode over a two-week test period. The measured and simulated energy flows are computed from system data for the same two week period for which thermal performance was discussed in Chapter 2. Selection of that interval and reduction of system data are discussed in the next section. Measured energy flows are computed with a program called RBM, listed in Appendix E. Simulated energy flows are computed with a similar program called RBS, also listed in Appendix E. The difference between RBM and RBS is that the latter ignores rock bed internal temperature data, using the TRNSYS rock bed model to simulate them. RBS also ignores rock bed outlet temperature, substituting the simulated downstream node rock temperature. As discussed in Chapter 1, that downstream rock temperature should represent the exit air temperature since Ntu_c for the test bed exceeds ten. Thus a comparison



*RBS does use T_{out} in an energy balance to determine a value for T_{in} (see text).

FIGURE 4.1.1 LONG-TERM SIMULATION TESTING METHOD

of the energy flow outputs of RBM and RBS should indicate the validity of the Infinite Ntu model.

4.2 Interval Selection and Data Reduction

The period chosen for long-term simulation testing is the longest uninterrupted interval with significant heating load after installation of backdraft dampers. The latter consideration is important in minimizing the effects of unknown thermosyphon losses as discussed in section 2.3. The selected interval is referred to as "Interval A". It is 322.4 hours long, and is bounded by tape runoffs, i.e. failure of personnel to change magnetic tapes on schedule.

Three special provisions are required to permit use of Interval A data. Flow resistance through the rock bed was changed by the addition of a fiberglass screen on the upper rock surface about half-way through the Interval. Thus the RBS program is supplied with two AS mode flowrates, and coded to use the lower value after the time corresponding to screen installation. (RBM uses furnace power to determine AS energy flows, so it does not need flowrate data.) Secondly, the SL mode velocity pressure transducer was accidentally left disconnected for the second half of Interval A. Thus RBM and RBS include coding to calculate SL mode velocity pressure based on a correlation with barometric pressure and air temperature, i.e. assuming constant average SL volume flowrate. Finally, as discussed in section 2.3, AS inlet air temperature must be corrected by balancing integrated air heat flow with integrated furnace power over

each ten minute data interval. The programs for calculating measured and simulated energy flows both include simple Euler integration of energy flowrates over time. Since data is available at ten minute intervals, the simple Euler method will yield the same results as the predictor-corrector integration scheme used in TRNSYS, as discussed earlier.

4.3 Analysis of Long-term Simulation Results

A summary of the outputs of programs RBM and RBS is shown in Table 4.3.1.

Table 4.3.1 Accuracy of Long-term Simulations

Energy quantities stored or discharged over two-week test period, by mode, GJ:

| | <u>CS</u> | <u>AS</u> | <u>SL</u> | <u>Losses</u> | <u>ΔU^4</u> | <u>Σ^5</u> |
|------------------------------------|--------------------------|-----------|-----------|-------------------|--------------------------------|------------------------------|
| Measurement | 1.98 to 2.36 avg=2.17 | 1.48 | 3.34 | 0.69 ² | ? ³ | -0.57 to -0.19 avg=-0.38 |
| Simulation 1 ¹ | 2.07 | 1.48 | 3.37 | 0.20 | -0.03 | 0.01 |
| <u>Simulation 1</u> Measurement | 1.15 to 0.92 avg=0.92 | 1.00 | 1.01 | | | |
| Simulation 2 | 2.09 | 1.48 | 3.23 | 0.50 | -0.04 | 0.12 |
| <u>Simulation 2</u> Measurement | 1.06 to 0.89 avg=0.96 | 1.00 | 0.97 | | | |

Notes: ¹"A" is without plenum losses, "B" includes them.

²Upper bound estimate

³Unknown -- see sec. 2.4.2

⁴ ΔU = Final internal energy - initial internal energy

⁵ Σ = CS + AS - SL - Losses - ΔU

The measured energy flows were discussed in sec. 2.4.2. The results shown for Simulation 1 are the energy flows entering and

leaving the rock bed which would be predicted by a TRNSYS model of the Arlington House, using weather data for Interval A. An energy balance on Simulation 1 closes within

$$\Sigma / (CS + AS) = 0.1\% ,$$

indicating that the simulation is probably valid. Comparison of Simulation 1 with measurement indicates that the simulated energy flows are within 5% of the measured energy flows. Since temperature profile information is available during the simulation, boundary losses and internal energy change can be estimated for Interval A. The internal energy decrease of 0.03 GJ corresponds to a decrease in bed temperature of 1.2°C (2.2°F) over the two-week test period. Boundary losses for Simulation 1 are calculated in the manner used in TRNSYS, considering losses only for wall surfaces in contact with rock. The 0.20 GJ loss shown is considered a lower bound on the true losses, since the upper plenum is often at the same temperature as the top node of the rock bed and includes a substantial wall area.

A second simulation, Simulation 2, has been performed to determine the effects of adding plenum losses to the rock bed losses normally considered by TRNSYS. The results of Simulation 2 are also shown in Table 4.3.1. The energy balance for Simulation 2 closes to within 3.1%. That is not a very good balance, but the reason for its magnitude remains unclear. The energy flows predicted by Simulation 2 are again within 5% of the measured flows. The loss value for Simulation 2 is 0.50 GJ, less than the upper bound estimate provided

by program RBM, and 2.5 times the loss predicted by TRNSYS. The difference between the losses predicted by Simulations 1 and 2 is 0.3 GJ, or 8% of the energy stored during Interval A.

The TRNSYS rock bed model simulates energy flows over long-term simulations with an accuracy of 5%. It may be desirable to extend the current loss calculation in the model to include the rock bed plenum chambers.

5.0 DESIGN OBSERVATIONS

Uniform air flow distribution is assumed as a basis for rock bed models, and intuitively seems desirable for optimum performance of storage and system. In areas of a rock bed receiving relatively high air flow, the thermocline will move downstream more rapidly than in the average and low-flow areas. If the flow in any area is so high that the thermocline often progresses to the end of the bed, that area will become saturated and will begin dumping energy into the exit air stream. The resulting increase in exit air temperature will then decrease the efficiency of the system's collectors.

Non-uniform flow distribution in the downward (charging) direction has been observed for the Arlington House rock bed, as described in section 2.3. A method for visualizing and quantifying flow distribution, the causes and effects of non-uniform flow distribution, and ways to avoid non-uniform flow distribution and leakage are discussed in this chapter.

5.1 Analysis of Flow Distribution

A technique for approximating flow distribution at the upstream face of a rock bed makes use of the infinite Ntu rock bed model. Given the initial temperature and physical parameters for a volume of rock at the upstream node, a finite difference method can be used iteratively to determine the flowrate through the volume required to produce the known final temperature in the volume. Such a method has been used to picture the flow distribution in the

current rock bed, and the results are illustrated in fig. 5.1.1. Note that this method is only an approximation, since Ntu_c is about four for any of the 80 equal volumes in the bed. Figure 5.1.1A is a bar graph showing the relative distribution of air flow to the sixteen stacks of the rock bed at the upper face and in a charging mode. Figure 5.1.1B shows the effect of spreading a screen of tightly-woven fiberglass fabric across the upper face in attempt to make the flow more uniform. Figure 5.1.1C indicates that somewhat less flow uniformity improvement was achieved by placing a set of diffuser vanes in front of the upper plenum inlet. Figure 5.1.1D illustrates flow distribution across the lower face of the bed in the discharging mode. It is considerably more uniform than the charging flow patterns shown in A and C, and comparable to the distribution shown in fig. 5.1.1B.

5.2 Causes and Effects of Non-uniform Flow

Maldistribution of flow through a rock bed may reduce system efficiency through several mechanisms: short circuiting, control "lead" or "lag", and energy dumping.

Short circuiting of air flow in either direction through a rock bed may occur if flow within a plenum is obstructed, the plenum is of insufficient height, or pressure drop through the rock bed is too low.

The Arlington House bed had a severe discharging short circuit before its lower plenum was modified during the summer of 1977.

Air was flowing directly between the lower and upper plenum ports,

Ⓐ TOP FACE - DOWNWARD FLOW
NO FLOW DISTRIBUTION AIDS

SCALE

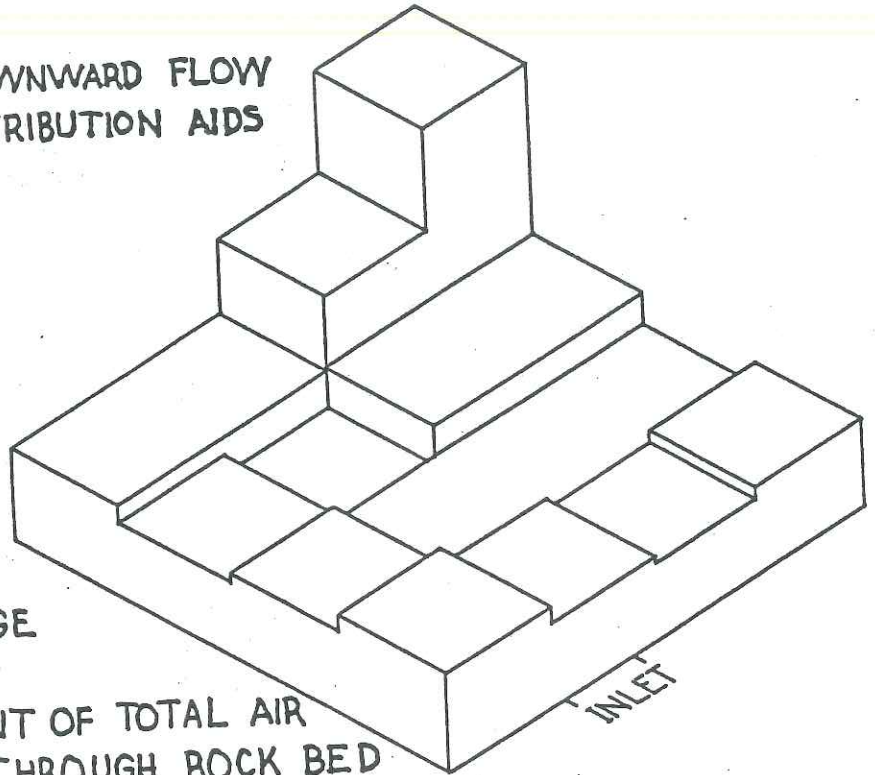
20

10

0

AVERAGE

PER CENT OF TOTAL AIR
FLOW THROUGH ROCK BED



Ⓑ TOP FACE - DOWNWARD FLOW
WITH SCREEN

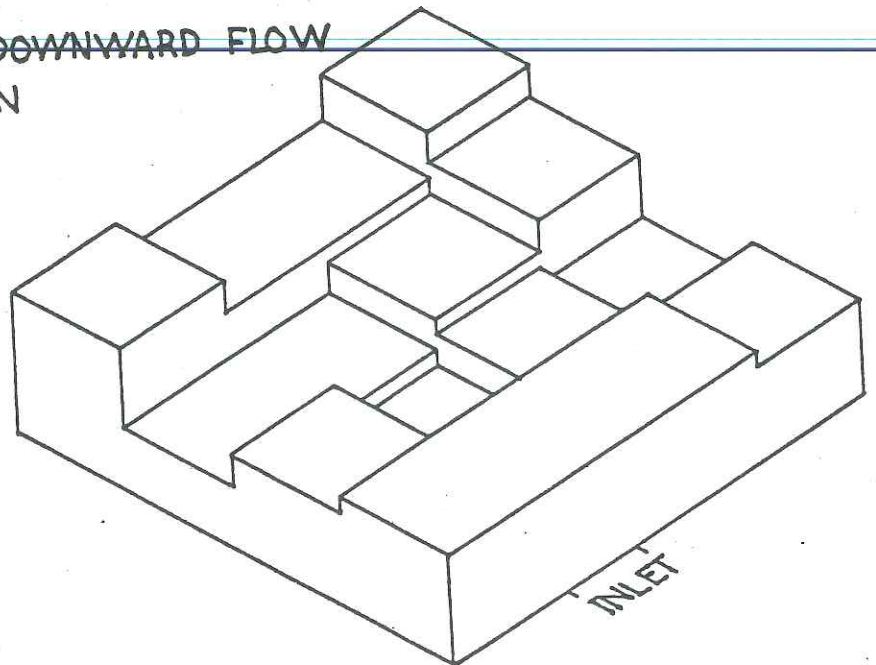
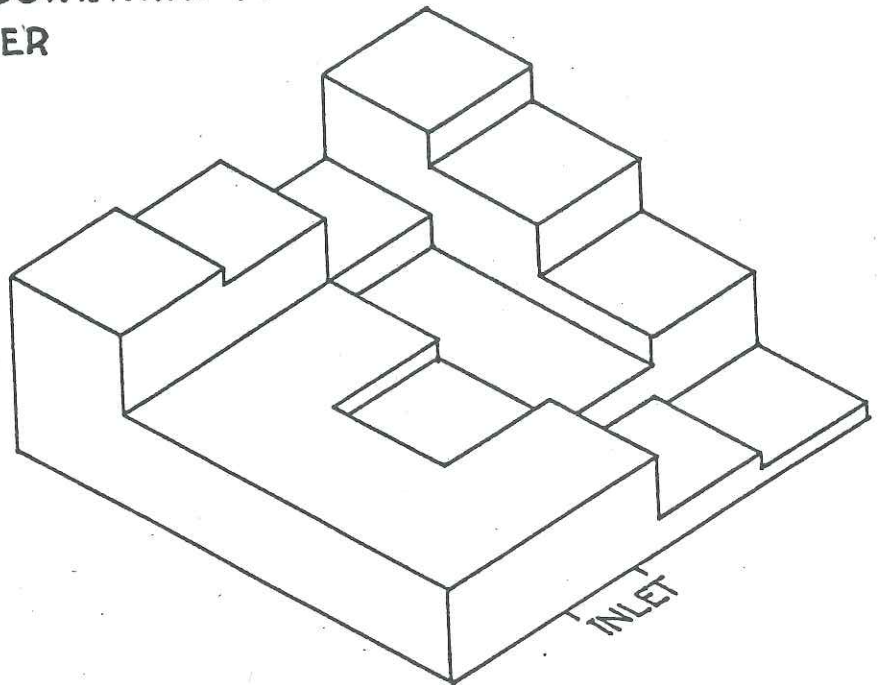


FIGURE 5.1.1 ROCK BED AIR FLOW DISTRIBUTION

© TOP FACE - DOWNWARD FLOW
WITH DIFFUSER



© BOTTOM FACE - UPWARD FLOW
NO FLOW DISTRIBUTION AIDS

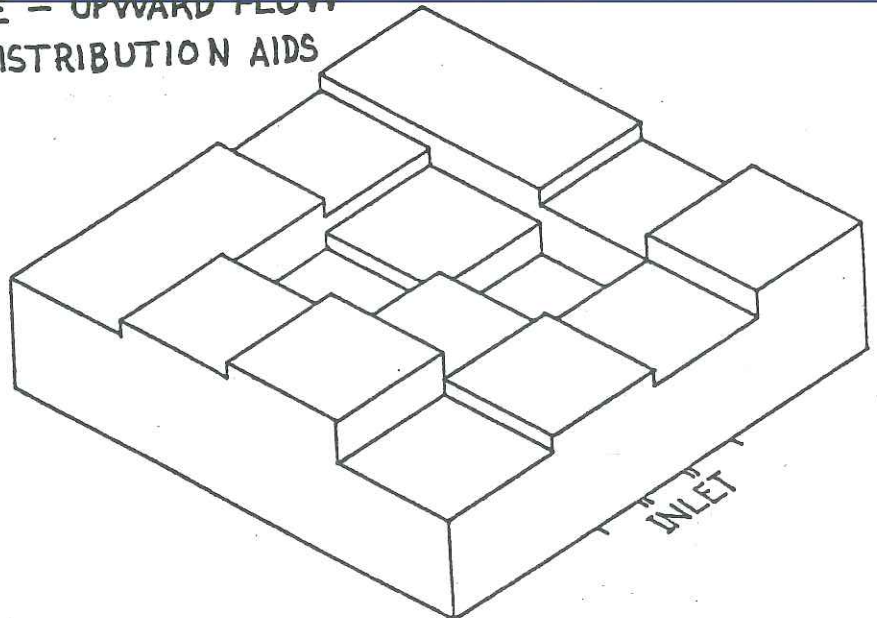


FIGURE 5.1.1 CONTINUED

along the west wall. This left most of the large quantity of energy stored in the bed inaccessible. This probably decreased the effective size of the bed in the discharging mode and required more parasitic power (fan operating time) in the SL mode than the ideal case. The problem was solved by removing the rocks, adding 4 in to the original 7 in height of the blocks supporting the wire mesh, and shifting the blocks from a rectangular array to a fan-shaped array centered on the inlet port. Thus the support blocks are used as a diffuser. As shown earlier, the discharging flow is now nearly uniform.

System efficiency may be decreased by non-optimal control due to placement of sensors in areas of relatively low or high air flow rate. Figure 5.2.1 illustrates a case of "control lag" observed for the Arlington bed. ~~Shown in the figure are the node-average~~ temperature profiles initially and after four hours of charging, and the temperature profile at the control sensors after four hours. The control sensor temperatures lag behind the node-average temperatures. Reference to figs. 2.2.1 and 5.1.1 indicates that this is probably due to the relatively low air flow entering the stack which includes the control sensors. In the Arlington System, the average of the five control sensor temperatures is compared to a manually set "bed average" temperature. The AS mode is activated if the average sensor temperature is below the set point when off-peak rates are in effect and there is no load. But the energy content of the bed is higher than desired when the control sensor

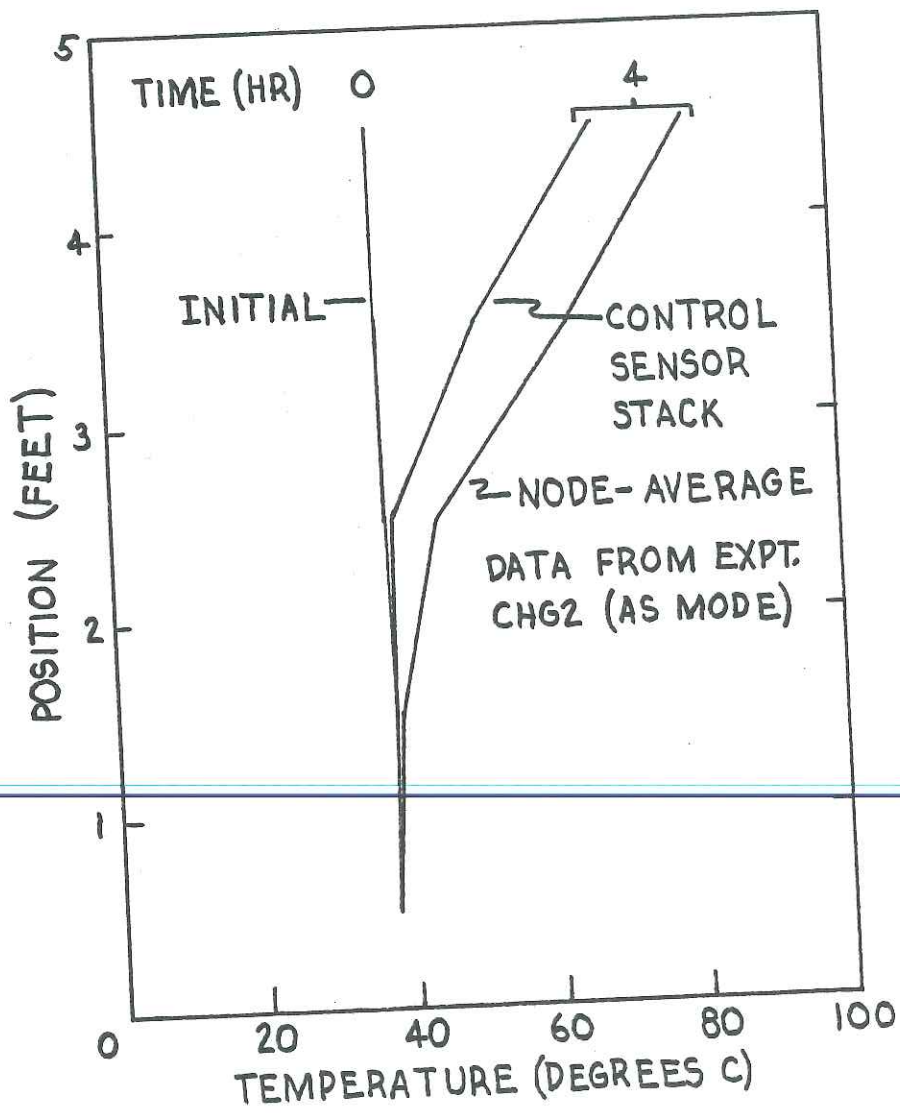


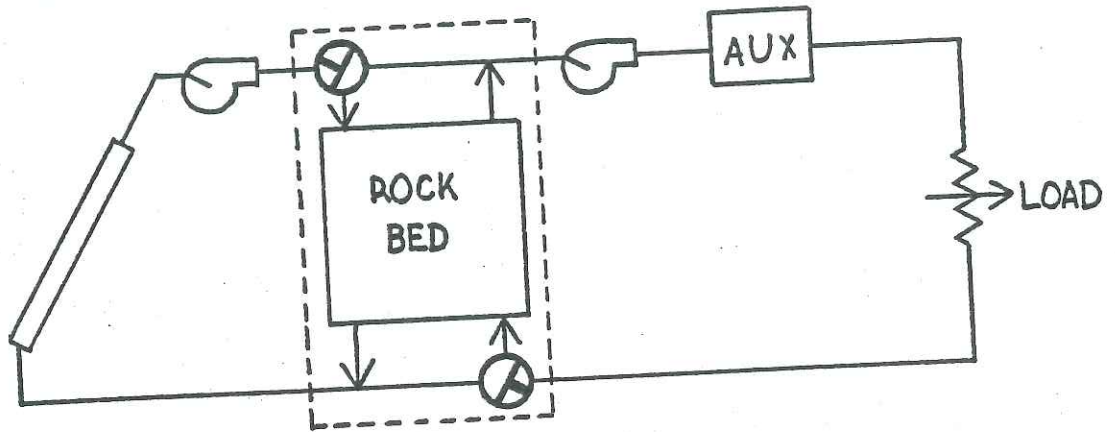
FIGURE 5.2.1 CONTROL LAG EFFECT

average temperature reaches the set point temperature. Thus losses through the bed enclosure may be increased and, if the bed were not oversized, collector losses might also increase as the collectors would receive unnecessarily warm supply air. In other beds, "control lead" might be a problem. Placement of a sensor in a high-flow area in the lower node of a bed might result in premature shutoff of the collector loop. Such control problems are best avoided by having uniform flow.

Energy dumping causes a reduction of system efficiency if a bed is undersized or if there is a great difference between flow distribution in the storage and discharging modes. Such a situation might occur in a rock bed with inadequate pressure drop and an undersized lower plenum. Assuming that the upper and lower plenum ports are located on the same wall, flow might then short circuit between them in the discharging mode and concentrate along the opposite wall in charging. Collectors would receive excessively hot air, and auxiliary heating would often be required in spite of the presence of considerable energy in the bed.

A simulation model is useful in observing the effect of non-uniform flow on energy dumping. Figure 5.2.2 is a schematic diagram of a system which can be simulated to illustrate this effect. First a simple air-based space heating system with series auxiliary is simulated with average Madison weather data. This indicates the ideal behavior of a system with uniform air flow in the rock bed. Next the system is simulated with a partitioned rock

SYSTEM I: WELL DISTRIBUTED AIR FLOW IN ROCK BED



SYSTEM II: POORLY DISTRIBUTED FLOW

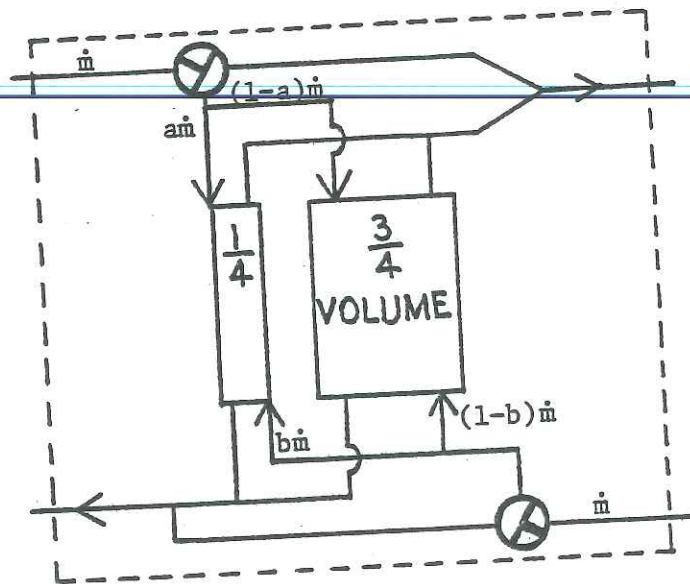


FIGURE 5.2.2 SYSTEM MODELS FOR SIMULATION OF NON-UNIFORM ROCK BED AIR FLOW

bed. The bed has the same total volume, height, and surface area, but is divided into two parts one-quarter and three-quarters of the original volume. The distribution of flow to these two parts may be varied independently for charging and discharging. Table 5.2.1 summarizes the results of several January simulations with these systems. (Results for March are similar.)

Table 5.2.1 Effect of Rock Bed Flow Distribution on System Performance: One-month Simulations

| System | Small Bed Flow | | System Efficiency | Fraction Solar |
|--------|----------------|-------------|-------------------|----------------|
| | Charging | Discharging | | |
| I | - | - | .46 | .42 |
| II | .25/.75 | .25/.75 | .46 | .42 |
| | .4/.6 | .25/.75 | .46 | .42 |
| | .9/.1 | .1/.9 | .39 | .35 |

$$\text{System efficiency} \equiv \frac{\text{Useful energy collected}}{\text{Total insolation}}$$

$$\text{Fraction solar} \equiv \frac{\text{Useful energy collected}}{\text{Load}}$$

The performance of System I can be matched with System II by directing 25% of the air flow to the small bed in both directions. This verifies the correct construction of the double-bed system model. If discharging flow is left uniform and 40% of the charging flow is directed to the small bed, system performance shows no significant change. This case is an approximation to the Arlington House rock bed, and indicates that the thermocline in the small bed rarely reaches the lower node. The final case is a severe maldistribution intended to display the mechanisms at work. Ninety per cent of the

charging flow is directed to the small bed, and 90% of the discharging flow is directed to the large bed. Table 5.2.1 shows the performance penalties resulting from such a maldistribution. System efficiency and solar fraction each decrease by seven percentage points.

5.3 Design for Uniform Flow

In section 5.2 it was shown that a rock bed with sufficiently poor flow distribution can be detrimental to system performance. Therefore achievement of uniform flow should be a consideration in rock bed design. Uniform flow through can be provided by choosing a rock diameter to optimize pressure drop (Δp) through the bed.

Optimization of pressure drop entails minimizing fan power by choosing the lowest Δp compatible with uniform flow. Flow distribution will probably be uniform if Δp is greater than the velocity pressure of the air entering a plenum at its inlet port. For instance, air enters the upper plenum of the Arlington House bed with a velocity pressure of 22.4 Pa (0.090 in H_2O) in the AS mode. In the same mode the pressure drop through the bed is 11.2 Pa (0.045 in H_2O) and, as shown in fig. 5.1.1A, flow is very poorly distributed. The flow distribution improvement resulting from the use of a fiberglass screen on top of the bed, shown in fig. 5.1.1B, is accompanied by an increase in pressure drop to 17.9 Pa (0.072 in H_2O). In the SL mode, air enters the lower plenum through a port with twice the area of the upper plenum port, with a velocity pressure of 1.99 Pa (0.008 in H_2O). Pressure drop through the bed in the SL mode is 2.49 Pa

(0.010 in H_2O), and air flow through the rock bed is fairly well distributed. These observations on the Arlington bed imply that uniform flow through a rock bed can be achieved by providing a pressure drop through the bed greater than the inlet air velocity pressure.

Pressure drop through a rock bed is a function of rock diameter and other parameters. Until recently there were no accurate correlations between rock diameter and pressure drop at the low Reynolds numbers typical of solar storage units. The correlation of Hollands and Pott [10], discussed in Chapter 1, does provide a good correlation between pressure drop and equivalent spherical rock diameter. Leflar [20] has noted that typical commercial screen size ranges (e.g. $d_{\min} - d_{\max}$) are approximately related to the equivalent spherical rock diameter used in the correlation by:

$$d_s = \frac{1}{3} (2d_{\min} + d_{\max}).$$

Hollands and Pott describe a means of estimating the rock surface area, A_s , for crushed (i.e., very angular) rock. For screened samples of mostly rounded rocks, it is adequate to assume spherical particles when calculating A_s .

Clearly inlet/outlet ports and plenum chambers should be designed to minimize velocity pressures. Ports should be designed to cover the maximum area over which inlet air can effectively be diffused, and plenum chambers should be designed with sufficient height to maintain low velocity pressure.

5.4 Leak Prevention

Excessive leakage from rock beds has plagued experimenters (refs. 15 and 16 , including the builders of the Arlington bed. Leakage to and from the bed was reduced to a low level during the reconstruction described in section 5.1, hence the materials and methods used deserve some mention.

The material used to seal the rock bed is sold as a high pressure duct sealer. It adheres permanently to almost any surface, cures to a high strength, and maintains its elasticity through prolonged exposure to high (e.g. 100°C) temperatures. In the reconstruction of the Arlington House rock bed, it was applied externally to all seams and corners. In new construction, a bead should be applied to the concrete floor just before sill placement, and to the edges of the back of each interior plywood panel for contact with the sill, studs, and top plate. Typical ceiling construction will permit sealing only on seams. These measures should help in avoiding a potentially severe problem.

RECOMMENDATIONS

The Arlington House rock bed should be tested and operated with two fiberglass screens on its top face. The use of two screens should improve the uniformity of air flow through the bed, making the temperatures at the control sensors and constantly monitored thermocouples more nearly representative of the node-average temperatures. The system pressure drop will be increased about 6.2 Pa (0.025 in H₂O) by the addition of each screen, but little change in parasitic power consumption will be detected since the overall system pressure drop is about 500 Pa (2 in H₂O).

Some means for accurately measuring inlet air temperature in the AS mode is required. The existing single thermocouple could be used if a mixing box could be fitted between the furnace and rock bed, but the resulting pressure drop increase could be prohibitive. Otherwise, several channels on the datalogger could be used to monitor an array of thermocouples.

A calorimetric determination of heat capacity as a function of temperature for the rocks in the bed would be useful.

It would also be of interest to place thermocouples in the top node to measure the temperature profile there in one- or two-inch depth increments, and the temperature gradients within rocks. (Thermocouples for the latter purpose are already located at mid-height in the bed, but the existence of significant gradients is most likely in the top node and in charging modes.)

Consideration should be given to including plenum convection losses in the TRNSYS rock bed model.

APPENDIX A: CALCULATION OF HEAT TRANSFER COEFFICIENT

Method

The calculation of h_v uses the solutions of Schumann [24] and the application technique of Furnas [8]. As explained by Löf and Hawley [21]:

"If the conditions of a particular heat transfer test are such that Schumann's assumptions are applicable, all of the data necessary for calculation of the temperature history of the fluid or solid are known or may be easily found, except the coefficient of heat transfer. The coefficient can therefore be determined by the ... method of Furnas. In the particular case where the fluid is a gas, the ratio of distance from entering end of the bed to fluid velocity through the bed, which is the term x/v_{fs} in the relation

$$Z = \frac{h_v}{c_b(1-\epsilon)} \left\{ \theta - \frac{x}{\epsilon v_{fs}} \right\},$$

is small in comparison with time and may be neglected. Time is therefore proportional to Z . the relation between

$$\frac{T_f - T_{b,0}}{T_{f,0} - T_{b,0}}$$

and the time θ , may be determined experimentally for any given test condition and location in the bed and the resulting curve may be compared with the Schumann curves which are plotted with Z as the abscissa. The value of Y for the curve which fits most closely the experimental results is then used to calculate the heat transfer coefficient, h_v , by using the relation

$$h_v = Y c_f v_{fs} / x \dots "$$

Procedure

- 1) Re-plot figs. 2, 4, and 6 of Furnas [8], Schumann curves for temperature history of gas, on a single semi-log plot. (See fig. A.1)
- 2) With the same logarithmic abscissa as used above, plot

$[(T_f - T_{b,0}) / (T_{f,0} - T_{b,0})]$ vs. θ for each of the five nodes, where

θ = time from start of test, hr (Use data from expt. CHG2),

T_f = temperature of air at time θ , °C,

$T_{b,0}$ = initial uniform temperature of bed = 38°C, and

$T_{f,0}$ = inlet air temperature = 88°C.

3) Slide plot (2) along plot (1) until the slope of the former most closely matches the slope of the latter for all values of dimensionless temperature difference. This implies a value for Y, by interpolation. (See fig. A.1)

4) Calculate h_v as $h_v = Y c_f v_{fs} / x$ where

c_f = heat capacity of air = 1.012 kJ/kg-°C,

v_{fs} = superficial fluid velocity = 178 m/hr, and

x = distance to node from top of bed, m

= 0.152, 0.457, 0.762, 1.07, and 1.07 for nodes 1 through 5.

Results

| Node | Y | h_v |
|------|-----|-------------------------------|
| 1 | 0.9 | 1020 kJ/hr-m ³ -°C |
| 2 | 7. | 2650 |
| 3 | 13. | 2950 |
| 4 | 16. | 2590 |
| 5 | 23. | 2910 |

Ignoring the value of h_v for node 1, since it seems to contradict the trend of the downstream nodes (whose temperature histories allow more accurate curve fits -- see fig. A.1), the average h_v is 2700 kJ/hr-m³-°C.

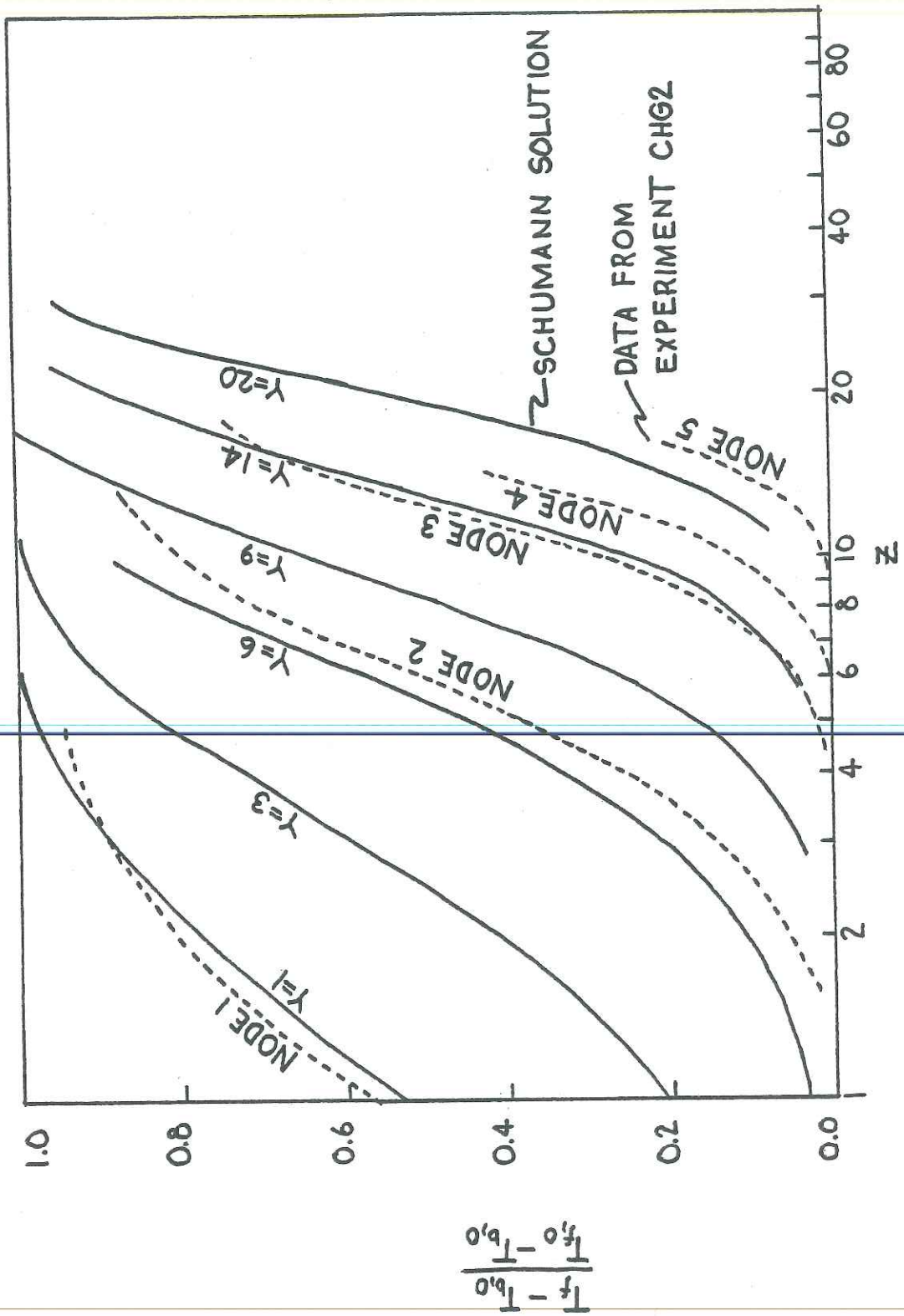


FIGURE A.1 CALCULATION OF HEAT TRANSFER COEFFICIENT

APPENDIX B: SPECIFICATIONS -- ARLINGTON HOUSE ROCK BED

| | | |
|--|---|--------------------|
| Altitude | 312.4±1.5 m (1025±5 ft) above MSL | |
| Length, N-S | 3.58 m (11'-8") | |
| Length, E-W | 3.40 m (11'-1") | |
| Flow Area | 12.2 m ² (131 ft ²) | |
| Flow length | 1.57 m (5'-2") | |
| Volume | 19.2 m ³ (677 ft ³) | |
| Void fraction | 0.428 | |
| Solid volume | 11.0 m ³ (388 ft ³) | |
| Specific gravity of solid | 2.73 | |
| Effective density | 1560 kg/m ³ (97.6 lbm/ft ³) | |
| Heat capacity of solid | See Chapter 1 | |
| Rock minimum diameter range | 1.9-4.1 cm (0.75-1.63 in) | |
| Rock geometric mean diameter | 2.9 cm (1.15 in) | |
| Surface area-to-volume ratio | 117 m ² /m ³ (35.8 ft ² /ft ³) | |
| Top plenum height | 0.43 m (17 in) | |
| Bottom plenum height | 0.28 m (11 in) | |
| <u>Flowrates: m³/hr (ft³/min) without screen or diffuser vanes</u> | | |
| Collector-to-storage (CS, downward flow) | 1410 (830) | |
| Auxiliary-to-storage (AS, downward flow) | 2070 (1220) | |
| Storage-to-load (SL, upward flow)* | 1280 (755) | |
| Superficial velocity (AS) | 0.0473 m/sec (9.31 ft/min) | |
| Particle velocity (AS) | 0.111 m/sec (21.8 ft/min) | |
| Particle dwell time (AS) | 14 sec | |
| <u>Pressure drop across rock bed, Pa (in H₂O)</u> | | |
| <u>Mode</u> | <u>without screen</u> | <u>with screen</u> |
| CS | 8.72 (0.035) | not measured |
| AS | 11.2 (0.045) | 17.9 (0.072) |
| SL* | 1.74 (0.007) | 2.49 (0.010) |

Support: 1.87 psf steel mesh with 0.8 x 3.5 in. openings on lintel blocks, 22% of mesh area in contact with blocks

*Subject to variation over time due to filter clogging.

APPENDIX C: NOMENCLATURE

| <u>Letter Symbols</u> | <u>SI units</u> |
|--|--|
| A Area | m^2 |
| A_s Total surface area of rocks in bed | m^2 |
| c Heat capacity | $\text{kJ/kg-}^\circ\text{C}$ |
| d_s Equivalent spherical diameter of bed particles = $[(6/\pi)(\text{net volume of particles}/\text{number of particles})]$ | m |
| D_h Hydraulic diameter of bed $=4LA_c/A_s$ | m |
| E Energy | GJ |
| f Friction factor | - |
| G Mass velocity of fluid through bed | kg/hr-m^2 |
| h Convective heat transfer coefficient | $\text{kJ/hr-m}^2\text{-}^\circ\text{C}$ |
| h_v Volumetric heat transfer coefficient $=h(A_s/V_b)$ | $\text{kJ/hr-m}^3\text{-}^\circ\text{C}$ |
| k Conductivity | $\text{kJ/hr-m-}^\circ\text{C}$ |
| L Flow length of bed | m |
| m Mass | kg |
| \dot{m} Mass flow rate of fluid through bed | kg/hr |
| N Number of nodes used in rock bed model | - |
| p Pressure (in $\text{H}_2\text{O} \times 249=$) | Pa |
| P Perimeter and Power | m kJ/hr |
| U Convective loss coefficient for rock bed walls and Internal Energy | $\text{kJ/hr-m}^2\text{-}^\circ\text{C}$ kJ |
| v Velocity | m/hr |
| v_{fs} Superficial fluid velocity $=\dot{m}/\rho_f A_{fr}$ | m/hr |
| V Volume | m^3 |
| x Position in rock bed | m |
| T Temperature | $^\circ\text{C}$ |
| <u>Greek Letters</u> | |
| Δ Change | - |
| ϵ Void fraction of packed bed | - |
| θ Time | hr |
| μ Viscosity of fluid | kg/m-hr |

| | | |
|--------|--|-----------------|
| ρ | Density | kg/m^3 |
| τ | Time constant for packed bed model $=\rho_b c_b (1-\epsilon)AL/\dot{m}c_f$ | hr |

Dimensionless Groups

| | |
|--------|--|
| Bi | Biot number $=hd_s/2k_b$ |
| Ntu | Number of heat transfer units $=h A_{fr} L/\dot{m}c_f$ |
| Pe | Peclet number $=Re_p Pr = v_f d_s \rho c_f / k_f$ |
| Re_b | Bed Reynolds number $=G_c D_c / \mu = 4G_c R_c / \mu$ |
| Re_p | Particle Reynolds number $=v_f d_s \rho / \mu$ |
| St | Stanton number $=h/\rho_f v c_f$ |

Subscripts

| | |
|-----|---|
| b | Bed material |
| c | Corrected; core, based on core area; critical |
| env | Surrounding environment |
| f | Heat transfer fluid; final |
| fr | Frontal, based on frontal area |
| i | Initial |
| in | Entering bed |
| m | Measured |
| out | Leaving bed |
| p | Furnace power |
| s | Simulated |

APPENDIX D: REFERENCES

1. Alanis, E., Saravia, L., and Rovetta, L., "Measurement of Rock Pile Heat Transfer Coefficients", Solar Energy, v 19, pp 571-572, (1977).
2. Clark, J.A., Nabozny, R.L., and Heetderks, J.H., "Rockbed: A Computer Program for Thermal Storage", Proceedings of the 1977 Annual Meeting, AS of ISES, p 17-17, Orlando, Florida, (1977).
3. Close, D.J., "Rock Pile Thermal Storage for Comfort Air Conditioning", Mechanical and Chemical Engineering Transactions of the Institution of Engineers, Australia, pp 11-19, May, (1965).
4. Duffie, J.A., and Beckman, W.A., Solar Energy Thermal Processes, Wiley-Interscience, New York, (1974).
5. Erdmann, D.R., "Thermal Performance of the Arlington Solar House", M.S. Thesis in Mechanical Engineering, University of Wisconsin, (1979).
6. Erdmann, D.R., and Persons, R.W., "The Arlington Solar House of the University of Wisconsin -- Madison", Proceedings of the Solar Heating and Cooling Systems Operational Results Conference,
7. Eshelman, W.D., Baird, C.D., and Mears, D.R., "A Numerical Simulation of Heat Transfer in Rock Beds", Proceedings of the 1977 Annual Meeting, AS of ISES, p 17-21, Orlando, (1977).
8. Furnas, C.C., "Heat Transfer From a Gas Stream to a Bed of Broken Solids", Transactions of the American Institute of Chemical Engineers, v 24, pp 142-193, (1930).
9. Handley, D., and Heggs, P.J., "The Effect of Thermal Conductivity of the Packing Material on Transient Heat Transfer in a Fixed Bed", International Journal of Heat and Mass Transfer, v 12, pp 549-570, (1969).
10. Hollands, K.G.T., and Pott, P., "Development and Testing of Evaporative Cooler Pads", Mechanical and Chemical Engineering Transactions of the Institution of Engineers, Australia, pp 66-72, November, (1971).
11. Hughes, P.J., "Design and predicted performance of the Arlington Solar House", M.S. Thesis in Mechanical Engineering, University of Wisconsin, (1975).

12. Hughes, P.J., Freeman, T.L., and Grunes, H., "Design of an Experimental Solar House Heating System", presented at the 1976 Winter Meeting, American Society of Agricultural Engineers.
13. Hughes, P.J., Klein, S.A., and Close, D.J., "Packed Bed Thermal Storage Models for Solar Air Heating and Cooling Systems", Journal of Heat Transfer, American Society of Mechanical Engineers, May, (1976).
14. Jeffreson, C.P., "Prediction of Breakthrough Curves in Packed Beds", American Institute of Chemical Engineers Journal, v 18, n 2, p 409, March (1972).
15. Jones, D., (National Bureau of Standards, Washington, DC), Personal Communication, November, 1978.
16. Karaki, S., Armstrong, P.R., and Bechtel, T.N., Evaluation of a Residential Solar Air Heating and Nocturnal Cooling System, Solar Energy Applications Laboratory, Colorado State University Fort Collins, (1977).
17. Kays, W.M., and London, A.L., Compact Heat Exchangers, McGraw-Hill New York, (1964).
18. Klein, S.A., "Mathematical Models of Thermal Storage", Proceedings of the Workshop on Solar Energy Storage and Sybsystems for the Heating and Cooling of Buildings, Virginia University, Charlottesville, (1975).
19. Kuhn, G.K., et al., Developing and Upgrading of Solar System Thermal Energy Storage Simulation Models, Technical Progress Report, DOE Contract EG-77-C-02-4482, Boeing Computer Services Co., Seattle, September (1978).
20. Leflar, J.A., "Some Useful Property Relationships for Rock, Air, and Packed Beds", Prepared as part of a technical information review for Project 7911, Fort Collins, Colorado, (1978).
21. Löf, G.O.G., and Hawley, R.W., "Unsteady-state Heat Transfer Between Air and Loose Solids", Industrial and Engineering Chemistry, v 40, n 6, pp 1061-1070, (1948).
22. Pfannkuch, H.O., and Edens, M.H., "Rock Properties for Thermal Energy Storage Systems in the 0 to 500°C Range", Proceedings of the 1977 Annual Meeting, AS of ISES, p 18-5, Orlando, (1977)

23. Riaz, M., "Transient Analysis of Packed-bed Thermal Storage Systems", Proceedings of the 1977 Annual Meeting, AS of ISES, p 18-5, Orlando, (1977).
24. Schumann, T.E.W., "Heat Transfer: a Liquid Flowing Through a Porous Prism", Journal of the Franklin Institute, v 208, pp 405-416, (1929).
25. University of Wisconsin Solar Energy Laboratory, TRNSYS, a Transient Simulation Program, Engineering Experiment Station Report 38-9, Madison, (1978).

APPENDIX E: COMPUTER PROGRAM LISTINGS

FDTIN

```

1 C THIS PROGRAM IS A DISTILLATION OF TRNSYS.TYPE10 WHICH INCLUDES ONLY
2 C STATEMENTS ESSENTIAL TO PREDICTION OF NODE TEMPERATURES. HYBRID IN-
3 C PUT AND OUTPUT SECTIONS ARE ATTACHED TO FACILITATE COMPARISON OF
4 C MODEL PREDICTIONS WITH DATA ON BEHAVIOR OF REAL ROCK BEDS.
5 C
6 C
7 C INPUT SECTION *****
8 C T AND DTDI ARRAYS DIMENSIONED LARGER THAN IN TYPE10 TO ALLOW USE OF
9 C TEMPERATURE GRADIENTS IN ESTIMATING FLOWRATE UNIFORMITY FROM REAL ROCK
10 C BED CHARGING DATA.
11 DIMENSION T(50),DTDI(50),OUT(15),INFO(9),TTOP(50),TBOT(50),
12 1FRNPNR(50)
13 C VARYING INLET TEMPERATURES, DEGREES C
14 READ(-,-)NT
15 READ(-,-)(TTOP(K),TBOT(K),FRNPNR(K),K=1,NT)
16 C SET FIRST-PASS FLAG
17 1 INFO(7)=-1
18 TIME=0.
19 DELTUT=0.
20 QENVT=0.
21 QTANKT=0.
22 WRITE(-,1091)
23 READ(-,-)N
24 IF(N,EQ,0)GO TO 4000
25 C AIR HEAT CAPACITY, KJ/KG-C
26 CP=1.01
27 C BED HEIGHT, M
28 IF(N,EQ,5)H=1.57
29 IF(N,EQ,1)H=0.314
30 C BED AREA, M**2
31 A=12.2

```

```

32 C BED PERIMETER, M
33 P=14.0
34 WRITE(,1092)
35 C ROCK HEAT CAPACITY, KJ/KG-C
36 READ(,)-)CFR
37 C BED EFFECTIVE DENSITY, KG/M**3
38 RHOR=1550.
39 C BED CONVECTIVE LOSS COEFFICIENT, KJ/HR-M**2-C
40 U=1.26
41 C BED EFFECTIVE THERMAL CONDUCTIVITY, KJ/HR-M-C
42 COND=0.45
43 WRITE(,1094)
44 C FLOW DIRECTION INDICATOR
45 READ(,)-)IFLOW
46 GO TO (10,20),IFLOW
47 10 CONTINUE
48 TIN=TTOP(1)
49 GO TO 25
50 CONTINUE
51 TIN=TBOT(1)
52 CONTINUE
53 WRITE(,1095)
54 C INLET TEMPERATURE CORRECTION TERM, DEGREES C
55 READ(,)-)TFIX
56 WRITE(,1096)
57 C FLOWRATE, KG/HR
58 READ(,)-)FLOW
59 C AVERAGE TEMPERATURE OUTSIDE BED, DEGREES C
60 TENV=15.
61 WRITE(,1097)
62 C INITIAL NODE TEMPERATURES, DEGREES C
63 READ(,)-)(I,I=1,N)
64 WRITE(,1098)
65 C DURATION OF SIMULATION, HRS
66 READ(,)-)DUR
67 1091 FORMAT(' NUMBER OF NODES=' )

```

```

68      1092 FORMAT(' ROCK HEAT CAPACITY (KJ/KG-C)=')
69      1094 FORMAT(' MODE CODE (1 FOR AS OR CS, 2 FOR SL)=')
70      1095 FORMAT(' CORRECTION TO INLET TEMPERATURE, DEGREES C')
71      1096 FORMAT(' FLOWRATE,KG/HR=')
72      1097 FORMAT(' INITIAL NODE TEMPERATURES, TOP FIRST,=')
73      1098 FORMAT(' DURATION OF SIMULATION, HRS=')
74      C
75      C *****
76      C COMPUTATION SECTION *****
77      C FIRST TIME THROUGH, CALCULATE INITIAL AVERAGE OF NODE TEMPS *****
78      2001 IF(INFO(7).GE.0) GO TO 100
79      T0=0.
80      OUT(15)=T0
81      DO 62 J=1,N
82      T0=T0+T(J)
83      62 CONTINUE
84      T0=T0/N
85      100 CONTINUE
86      NMI=N-1
87      VOL=AXH
88      DELTX=H/N
89      UA=U*P*DELTX
90      EFCOND=COND**DELTX
91      CAPN=VOL*CFR**RHOR
92      CAPN=CAP/N
93      FC=FLOW*CP
94      GO TO(11,12),IFLOW
95      C CHARGING
96      11 CONTINUE
97      QENV=UA*(T(1)-TENV)
98      QTANK=0.
99      DTDI(1)=(FC*(TIN-T(1))-QENV-EFCOND*(T(1)-T(2)))/CAPN
100     GO TO 22
101     C DISCHARGING
102     12 CONTINUE
103     QENV=UA*(T(N)-TENV)

```

```

104 QTANK=FC*(T(1)-TIN)
105 DTD(T(N))=(FC*(TIN-T(N))-QENV+EFCOND*(T(N-1)-T(N)))/CAPN
106
107 22 CONTINUE
108 C SKIP INTERMEDIATE NODE CALCULATIONS FOR ONE- OR TWO-NODE BEDS.
109 IF(N.LE.2) GO TO 44
110 DO 8 J=2,NM1
111 GO TO (5,6),IFLOW
112 5 K1=J-1
113 K2=J
114 GO TO 7
115 6 K1=N-J+2
116 K2=N-J+1
117 7 CONTINUE
118 QENV=QENV+UA*(T(K2)-TENV)
119 DTD(T(K2))=(FC*(T(K1)-T(K2))-UA*(T(K2)-TENV)
120 1+EFCOND*(T(K2-1)-T(K2))+EFCOND*(T(K2+1)-T(K2)))/CAPN
121 8 CONTINUE
122 44 CONTINUE
123 C SKIP SECOND EXTERIOR NODE CALCULATION FOR ONE-NODE SYSTEMS.
124 IF(N.EQ.1) GO TO 4
125 GO TO (31,32),IFLOW
126 31 CONTINUE
127 DTD(T(N))=(FC*(T(N-1)-T(N))-UA*(T(N)-TENV)+EFCOND*(T(N-1)-T(N)))/CAP
128 1N
129 QENV=QENV+UA*(T(N)-TENV)
130 GO TO 33
131 32 CONTINUE
132 DTD(T(1))=(FC*(T(2)-T(1))-UA*(T(1)-TENV)-EFCOND*(T(1)-T(2)))/CAPN
133 QENV=QENV+UA*(T(1)-TENV)
134 33 CONTINUE
135 4 CONTINUE
136 TBAR=0.
137 DO 119 J=1,N
138 TBAR=TBAR+T(J)
139 TBAR=TBAR/N
140 DELTU=CAP*(TBAR-OUT(15))

```

```

140 C
141 C EXEC SECTION *****
142 C REMOVE FIRST-PASS FLAG *****
143 C
144     INFO(7)=1
145     DO 3003 J=1,N
146     C TIMESTEP=1/6 HR=10 MINUTES
147     T(J)=T(J)+(DTD(J)/6.)
148     3003 CONTINUE
149     QENV=QENV+QENV*1./6.
150     QTANK=QTANK+QTANK*1./6.
151     DELTUT=DELTUT+DELTU*1./6.
152     TIME=TIME+1./6.
153     IF(TIME.GE.DUR)GO TO 405
154     GO TO(3005,3006),IFLOW
155     3005 M=1+INT(TIME/0.333)
156     TIN=TTOP(M)+TFIX
157     GO TO 3007
158     3006 M=1+INT(TIME/0.333)
159     TIN=TROT(M)+TFIX
160     3007 GO TO 2001
161 C
162 C OUTPUT SECTION *****
163 C
164     405 WRITE(-,4001)
165     WRITE(-,4002)((I,T(I)),I=1,N)
166     IF(IFLOW.NE.2)GO TO 409
167     WRITE(-,4003)QTANK
168     409 CONTINUE
169     WRITE(-,4004)DELTUT
170     WRITE(-,4005)QENV
171     WRITE(-,4006)
172     GO TO 1
173     4000 WRITE(-,4007)
174     4001 FORMAT(//)
175     4002 FORMAT(' T(',I2,')=',F5.1)

```

```

176 4003 FORMAT(' QTANK='E14.7)
177 4004 FORMAT(' DELTU='E14.7)
178 4005 FORMAT(' GENV='E14.7)
179 4006 FORMAT(////)
180 4007 FORMAT(' NO NODES, NO ANSWERS. BYE!')
181 STOP
182 END

```

RBM

```

1 C THIS PROGRAM USES MEASURED DATA TO CALCULATE ENERGY TURNOVER BY
2 C MODE FOR THE ARLINGTON HOUSE ROCK BED.
3 C FOR AN EXPLANATION OF THE CODING USED IN THIS PROGRAM, REFER
4 C TO ITS COMPANION PROGRAM, "RBS".
5 READ('-',-)LUNT,NFILES,LSTOPT
6 DO 600 IFILES=1,NFILES
7 READ(LUNT,'-')NSCANS
8 DO 510 ISCANS=1,NSCANS
9 READ(LUNT,405)TNEW,CH5,CH12,CH13,CH14,CH18,CH28,CH29,CH40
10 405 FORMAT(F11.4/41X,F7.3/16X,3(1X,F7.4),25X,F7.3/64X,2(1X,F7.1)//
11 &1X,F7.3/)
12 410 IF(IFILES.EQ.1.AND.ISCANS.EQ.1)GO TO 505
13 IF(C400.LT.0.229.OR.C400.GT.0.239)GO TO 420
14 IF(CH40.GE.0.229.AND.CH40.LE.0.239)GO TO 415
15 PB=(27.771+0.04456*(C130)*0.491 @ LBF/IN2
16 RHO=144.*PB/(53.34*(C290+273.0)*1.8) @ LBM/FT3
17 PV=200.*(C120-0.0016)/394.5 @ IN H20
18 IF(PV.LT.0.)PV=0.
19 V=1096.5*SQRT(PV/RHO) @ FT/MIN
20 FLOW=RHO*V*0.6667/(2.2046*60.) @ KG/SEC
21 ECS=ECS+(FLOW*1.012*(C280-C290)*(TNEW-TOLD))*3600. @ KJ
22 RHOA=144.*PB/(53.34*(C280+273.0)*1.8)
23 PVA=200.*(C130+0.0148)/398.8
24 IF(PVA.LT.0.)PVA=0.
25 VA=1096.5*SQRT(PVA/RHOA)

```

```

26 FLOW=RHOA*VA*0.6667/(2.2046*60.)
27 ECSA=ECSA+(FLOW*1.012*(C280-C290)*(TNEW-TOLD))*3600.
28 GO TO 420
29 PB=(27.771+0.04456*CH18)*0.491 @ LBF/IN2
30 RHO=144.*PB/(53.34*(CH28+273.0)*1.8) @ LBM/FT3
31 PV=200.*(CH12-0.0016)/394.5 @ IN H2O
32 IF(PV,LT.0.)PV=0.
33 V=1096.5*SQRT(PV/RHO) @ FT/MIN
34 FLOW=RHO*V*0.6667/(2.2046*60.) @ KG/SEC
35 ECS=ECS+(FLOW*1.012*(CH28-CH29)*(TNEW-TOLD))*3600. @ KJ
36 RHOA=144.*PB/(53.34*(CH28+273.0)*1.8)
37 PVA=200.*(CH13+0.0148)/398.8
38 IF(PVA,LT.0.)PVA=0.
39 VA=1096.5*SQRT(PVA/RHOA)
40 FLOW=RHOA*VA*0.6667/(2.2046*60.)
41 ECSA=ECSA+(FLOW*1.012*(CH28-CH29)*(TNEW-TOLD))*3600.
42 IF((CH40,GE.1.860,AND,CH40,LE.1.870)
43 &.OR,(C400,GE.1.860,AND,C400,LE.1.870))GO TO 430
44 GO TO 440
45 DAY=TNEW/24.
46 FRAC=DAY-AINT(DAY)
47 IF(FRAC,GT.0.3263,AND,FRAC,LT.0.9238)GO TO 440
48 E=1439.*((-CH5)-0.018-0.014*(TNEW-TOLD))*1.02 @ KJ
49 PWR=E/((TNEW-TOLD)*3600.) @ KWH
50 IF(PWR,LT.0.)GO TO 440
51 IF(PWR,GT.45.)E=45.*(TNEW-TOLD)*3600.
52 EAS=EAS+E @ KJ
53 IF(C400,LT.3.902,OR,C400,GT.3.912)GO TO 500
54 IF(CH40,GE.3.902,AND,CH40,LE.3.912)GO TO 445
55 PB=(27.771+0.04456*CH18)*0.491 @ LBM/FT3
56 IF(TNEW,GT.10579.85)GO TO 480
57 RHO=144.*PB/(53.34*(C280+273.0)*1.8) @ LBM/FT3
58 PV=200.*(C140-0.0007)/245.5 @ IN H2O
59 IF(PV,LT.0.)PV=0.
60 V=1096.5*SQRT(PV/RHO) @ FT/MIN
61 FLOW=RHO*V*0.4444/(2.2046*60.) @ KG/SEC

```

```

62 ESL=ESL+(FLOW*1.012*(C280-C290)*(TNEW-TOLD))*3600. @ KJ
63 GO TO 500
64 C140=5.21*PB/((C280+273.)*0.491)
65 GO TO 470
66 PB=(27.771+0.04456*CH18)*0.491 @ LBM/FT3
67 IF(TNEW.GT.10579.85)GO TO 460
68 RHO=144.*PB/(53.34*(CH28+273.)*1.8) @ LBM/FT3
69 PV=200.*(CH14-0.0007)/245.5 @ IN H2O
70 IF(PV.LT.0.)PV=0.
71 V=1096.5*SQRT(PV/RHO) @ FT/MIN
72 FLOW=RHO*V*0.4444/(2.2046*60.) @ KG/SEC
73 ESL=ESL+(FLOW*1.012*(CH28-CH29)*(TNEW-TOLD))*3600. @ KJ
74 GO TO 500
75 460 CH14=5.21*PB/((CH28+273.)*0.491)
76 GO TO 450
77 C ASSUME AVERAGE ROCK BED TEMPERATURE IS 45C, SURROUNDINGS 15C
78 500 UALOSS=UALOSS+1.26*5d.2*(45-15)*(TNEW-TOLD) @ KJ
79 505 TOLD=TNEW
80 C50=CH5
81 C120=CH12
82 C130=CH13
83 C140=CH14
84 C180=CH18
85 C280=CH28
86 C290=CH29
87 C400=CH40
88 CONTINUE
89 READ(LUNT,405,END=520)DUMMY
90 CALL CLOSE(LUNT,0)
91 CALL IOTFSF(LUNT)
92 CONTINUE
93 XLOSS=ECS+EAS-ESL-UALOSS
94 XLOSSA=ECSA+EAS-ESL-UALOSS
95 IF(LSTOPT.NE.0)WRITE(6,610)
96 610 FORMAT(/' ECS=ENERGY STORED IN CS MODE BASED ON FLOW TO COLLECTORS
97 &' /

```

```

98 & ECSA=ENERGY STORED IN CS MODE BASED ON FLOW FROM COLLECTORS' /
99 & EAS=ENERGY STORED IN AS MODE BASED ON ELECTRICAL USAGE' /
100 & ESL=ENERGY WITHDRAWN IN SL MODE' /
101 & UALOSS=ESTIMATED UA ENERGY LOSS' /
102 & XLOSS=ECS+EAS-ESL-UALOSS' /
103 & XLOSSA=ECSA+EAS-ESL-UALOSS' /
104 WRITE(6,620)
105 WRITE(6,630)ECS,ECSA,EAS,ESL,UALOSS,XLOSS,XLOSSA
106 620 FORMAT(/, ' ENERGY QUANTITIES, KILOJOULES:',
107 & /1X,5X,'ECS',7X,'ECSA',6X,'EAS',7X,'ESL',6X,'UALOSS',3X,
108 & 'XLOSS',3X,'XLOSSA')
109 630 FORMAT(1X,7(2X,E8.3)/)
110 STOP
111 END

```

RBS

```

1 C THIS PROGRAM USES MEASURED FLOWRATE AND INLET TEMPERATURE DATA
2 C TO PREDICT ENERGY TURNOVER BY MODE FOR THE ARLINGTON HOUSE ROCK
3 C BED. ASSIGN SDF FILE "7." FOR USE BY THIS PROGRAM.
4 C
5 C CH ARRAY STORES INPUT DATA
6 C DTTD ARRAY STORES TEMPERATURE CHANGE RATES FOR BED NODES
7 C DIMENSION T(10),CH(40,2),DTDT(10)
8 C NFILES=NUMBER OF DAYS TO BE SIMULATED
9 C READ(,-)LUNT,NFILES,IUAOPT
10 C N=NUMBER OF NODES IN BED MODEL
11 C CP=HEAT CAPACITY OF AIR, NJ/KG-C
12 C H=HEIGHT OF BED, M
13 C A=FLOW AREA OF BED, M2
14 C P=PERIMETER OF BED, M
15 C CPR=HEAT CAPACITY OF ROCK, KJ/KG-C
16 C RHOR=EFFECTIVE DENSITY OF ROCK (INCLUDING VOIDS), KG/M3
17 C U=CONVECTIVE LOSS COEFFICIENT OF ROCK BOX, KJ/HR-M2-C
18 C COND=EFFECTIVE THERMAL CONDUCTIVITY OF ROCK BED, KJ/HR-M-C

```

```

19 C TENV=AVERAGE TEMPERATURE OF BED SURROUNDINGS, C
20 C T(K)=TEMPERATURE OF NODE K, C
21 C >>>PARAMETERS NOT NORMALLY CONSIDERED IN TRNSYS:
22 C ATP,ABP=TOP AND BOTTOM PLENUM AREAS
23   READ(7,-)N,CP,H,A,P,CPR,RHOR,U,COND,TENU,(T(K),K=1,N),
24   1ATP,ABP
25 C INITIAL INTERNAL ENERGY :
26   DO 100 NN=1,N
27   100 USTRT=USTRT+(A*(H/N)*RHOR*CP*RT(NN))
28 C FIXED QUANTITIES
29   VOL=AXH @ M3
30   DELTX=H/N @ M
31   UA=UXP*DELTX @ KJ/HR-C
32   UAT=UX*ATP
33   UAB=UX*ABP
34   IF(IUAOPT.GE.1)GO TO 150
35   UAT=0.
36   UAB=0.
37   150 EFCOND=COND*A/DELTX @ KJ/HR-C
38   CAP=VOL*CFR*RHOR @ KJ/C, WHOLE BED
39   CAPN=CAP/N @ KJ/C, SINGLE NODE
40   NM1=N-1
41   WRITE(6,170)
42   170 FORMAT(/, TEMPERATURE PROFILES AT START, MIDNIGHT SCANS, AND FINIS
43   &,' )
44 C DAY LOOP STARTS HERE
45   DO 600 IFILES=1,NFILES
46 C PRINT TEMPERATURE PROFILE AS DAY BEGINS
47   WRITE(6,200)(T(K),K=1,N)
48   200 FORMAT(1X,10(2X,F5.1))
49   READ(LUNT,-)NSCANS
50 C SCAN, OR INTERVAL, LOOP STARTS HERE
51   DO 510 ISCANS=1,NSCANS
52 C LOAD DATA FOR END OF PRECEDING INTERVAL
53   READ(LUNT,405)TNEW,CH(5,2),CH(12,2),CH(13,2),CH(14,2),CH(18,2),
54   1CH(28,2),CH(29,2),CH(40,2)

```

```

55 405 FORMAT(F11.4/41X,F7.3/16X,3(1X,F7.4),25X,F7.3/64X,2(1X,F7.1)//
56 81X,F7.3/)
57 C SKIP FIRST SET OF ENERGY CALCULATIONS, SINCE DATA FOR BOTH ENDS OF
58 C FIRST INTERVAL WILL BE REQUIRED
59 IF(IFILES.EQ.1.AND.ISCANS.EQ.1)GO TO 505
60 C ASSUME THAT MODE CHANGES AT END OF INTERVAL, I.E. DATA USED WILL BE
61 C THAT FOR START OF INTERVAL
62 I=1
63 C IF MODE ISN'T C/S AT START OF INTERVAL, PROCEED TO NEXT SECTION TO
64 C SEE WHETHER IT IS A/S
65 IF(CH(40,1).LT.0.229.OR.CH(40,1).GT.0.239)GO TO 420
66 C IF MODE IS C/S AT START AND END OF INTERVAL, USE DATA FROM
67 C END OF INTERVAL
68 IF(CH(40,2).GE.0.229.AND.CH(40,2).LE.0.239)I=2
69 C SET "DOWNWARD FLOW" SIGNAL FOR FD SUBROUTINE
70 IFLOW=1
71 C CALCULATE BAROMETRIC PRESSURE
72 PB=(27.771+0.04456*CH(18,1))*0.491 @ LBF/IN2
73 C CALCULATE DENSITY OF AIR
74 RHO=144.*PB/(53.34*(CH(28,I)+273.0)*1.8) @ LBM/FT3
75 C CALCULATE VELOCITY PRESSURE
76 PV=200.*(CH(13,I)+0.0148)/398.8 @ IN H2O
77 C GUARD AGAINST ERROR TERMINATION IN SQRT FUNCTION
78 IF(PV.LT.0.)PV=0.
79 C CALCULATE AIR VELOCITY
80 V=1096.5*SQRT(PV/RHO) @ FT/MIN
81 C CALCULATE MASS FLOW RATE
82 FLOW=60.*RHO*V*0.6667/2.2046 @ KG/HR
83 C SEE EXPLANATION OF TFIX IN A/S SECTION BELOW
84 TFIX=0.
85 CALL FD @ INTERNAL SUBROUTINE SEE BELOW
86 C CALCULATE C/S ENERGY STORED OVER THE INTERVAL BASED ON KNOWN
87 C FLOWRATE AND INLET TEMPERATURE. USE BOTTOM NODE TEMPERATURE
88 C PREDICTED BY FD AS THE OUTLET TEMPERATURE.
89 ECS=ECS+(FLOW*CP*(CH(28,I)-T(N))*(TNEW-TOLD)) @ KJ
90 I=1

```

```

91 IF(CH(40,1),LT,1.860,OR,CH(40,1),GT,1.870)GO TO 440
92 IF(CH(40,2),GE,1.860,AND,CH(40,2),LE,1.870)I=2
93 IFLOW=1
94 C IGNORE A/S SEQUENCES OCCURRING DURING ON-PEAK HOURS
95 DAY=TNEW/24.
96 FRAC=DAY-AINT(DAY)
97 IF(FRAC.GT,0.3263,AND,FRAC.LT,0.9238)GO TO 440
98 C FOR A/S SEQUENCES SHOWING NO POWER CONSUMPTION (E.G. FLOWRATE
99 C EXPERIMENT SEQUENCES), BYPASS TO CALCULATION OF NEW TEMPERATURE
100 C PROFILE DUE TO UA LOSS AND CONDUCTION
101 E=1439.*((-CH(5,I))-0.018-0.014*(TNEW-TOLD))*1.02 @ KJ
102 IF(E.LT,0.)GO TO 430
103 PB=(27.771+0.04456*CH(18,I))*0.491 @ LBF/IN2
104 RHO=144.*PB/(53.34*(CH(29,I)+273.0))*1.8 @ LBM/FT3
105 VFLOW=2070. @ M**3/HR
106 C SCREEN INSTALLED MARCH 16, 1978, 3 P.M.
107 IF(TNEW.GT,10551.0)VFLOW=1950. @ M3/HR
108 FLOW=VFLOW*RHO*16.018 @ KG/HR
109 TFIX IS A CORRECTION REQUIRED FOR THE A/S INLET PORT TEMPERATURE DUE
110 C TO PROXIMITY OF THERMOCOUPLE AND HEATING ELEMENTS, BASED ON BALANCE
111 C OVER INTERVAL OF FLOW AND ELECTRICAL ENERGIES
112 TFIX=--(E-(FLOW*CP*(TNEW-TOLD)*(CH(28,I)-CH(29,I))))/
113 1(FLOW*CP*(TNEW-TOLD)) @ DEGREES C
114 CALL FD
115 EAS=EAS+(FLOW*CP*(CH(28,I)-TFIX-T(N))*(TNEW-TOLD)) @ KJ
116 GO TO 440
117 FLOW=0.0
118 CALL FD
119 I=1
120 IF(CH(40,1),LT,3.902,OR,CH(40,1),GT,3.912)GO TO 500
121 IF(CH(40,2),GE,3.902,AND,CH(40,2),LE,3.912)I=2
122 IFLOW=2
123 PB=(27.771+0.04456*CH(18,I))*0.491 @ LBF/IN2
124 CH14=CH(14,I)
125 IF(TNEW.LT,10579.85)GO TO 470
126 CH14=5.21*PB/((CH(28,I)+273.0)*0.491) @ VOLTS

```

```

127
128
129
130
131
132
133
134
135
136
137
138
139
140
141
142
143
144
145
146
147
148
149
150
151
152
153
154
155
156
157
158
159
160
161
162

470 RHO=144.*PB/(53.34*(CH(28,I)+273.)*1.8) @ LBM/FT3
    PV=200.*(CH14-0.0007)/245.5 @ IN H2O
    IF(PV.LT.0.)PV=0.
    V=1096.5*SQRT(PV/RHO) @ FT/MIN
    FLOW=60.*RHO*V*.4444/2.2046 @ KG/HR
    CALL FD

490 ESL=ESL+FLOW*CP*(T(1)-CH(29,I))*(TNEW-TOLD)
C CALCULATE UA LOSS AND CONDUCTION EFFECTS ON TEMPERATURE PROFILE IF
C MODE IS C/L OR IDLE FOR THE INTERVAL
500 IF(CH(40,1).GE.1.141.AND.CH(40,1).LE.1.151
    1.OR.CH(40,1).GE.4.993.AND.CH(40,1).LE.5.003)GO TO 501
    GO TO 505
501 FLOW=0.0
    IFLOW=1
    I=1
    CALL FD

C DATA FROM END OF CURRENT INTERVAL BECOMES DATA FOR START OF NEXT
C INTERVAL.
505 TOLD=TNEW
    DO 506 NCH=5,40
506 CH(NCH,1)=CH(NCH,2)
510 CONTINUE
C USE READ WITH END OPTION TO TERMINATE DAY
    READ(LUNT,405,END=520)DUMMY
C ZERO OPTION ON CLOSE ROUTINE PREVENTS AUTOMATIC TAPE REWIND
520 CALL CLOSE(LUNT,0)
C SPACE TAPE PAST EOF TO START NEXT DAY
    CALL IOTPSF(LUNT)
600 CONTINUE
C PRINT FINAL TEMPERATURE PROFILE
    WRITE(6,200)(T(K),K=1,N)
C FINAL INTERNAL ENERGY
    DO 610 NN=1,N
610 UFIN=UFIN+(A*(H/N)*RHOR*CFR*(NN)) @ KJ
        DELTU=UFIN-USTRT
        XLOSS=ECS+EAS-ESL-UALOSS-DELTU

```

```

199 1+EFCOND*(T(K2-1)-T(K2))+EFCOND*(T(K2+1)-T(K2))/CAPN
200 8 CONTINUE
201 44 CONTINUE
202 C SKIP SECOND EXTERIOR NODE CALCULATION FOR ONE-NODE SYSTEMS
203 IF(N.EQ.1)GO TO 4
204 GO TO (31,32), IFLOW
205 C CHARGING, BOTTOM NODE
206 31 CONTINUE
207 DTD(T(N))=(FC*(T(N-1)-T(N))-UA*(T(N)-TENV))
208 1+EFCOND*(T(N-1)-T(N))/CAPN
209 QENV=QENV+(UA+UAB)*(T(N)-TENV)
210 GO TO 33
211 C DISCHARGING, TOP NODE
212 32 CONTINUE
213 DTD(T(1))=(FC*(T(2)-T(1))-UA*(T(1)-TENV)-EFCOND*(T(1)-T(2)))/CAPN
214 QENV=QENV+(UA+UAT)*(T(1)-TENV)
215 33 CONTINUE
216 4 CONTINUE
217 UALOSS=UALOSS+QENV*(TNEW-TOLD)
218 DO 119 J=1,N
219 T(J)=T(J)+DTD(J)*(TNEW-TOLD)
220 RETURN
221 END

```